Lappeenranta University of Technology

School of Technology

Master's Degree Program in Chemical and Process Engineering

Maan Hafiz Muhammad Fazeel

Influence of reactant absorption and dissolution in heterogeneous precipitation processes

Examiner: Professor Marjatta Louhi-Kultanen

Supervisor: M.Sc. Bing Han

ACKNOWLEDGEMENTS

I would like to say thanks to Almighty ALLAH for his blessing.

This thesis is accomplished with the kind support of Professor Marjatta Louhi-Kultanen. Professor Marjatta Louhi-Kultanen is being very kind throughout this research. I highly appreciate the help of M.Sc. Bing Han too.

I would also like to say thanks to LUT stuff members for their concern throughout my studies duration. Lastly I would like to gratitude my family for their support and pray.

I dedicate this thesis research to my family.

Abstract

Lappeenranta University of Technology
School of Technology
Master's Degree Program in Chemical and Process Engineering
Maan Hafiz Muhammad Fazeel
Influence of reactant absorption and dissolution in heterogeneous precipitation processes
2014

82 pages, 39 figures, 13 tables and 2 appendices.

Examiner: Professor Marjatta Louhi-Kultanen

Keywords: Precipitation, crystallization, and oxygen mass transfer coefficient.

In this research work, the aim was to investigate the volumetric mass transfer coefficient [k_La] of oxygen in stirred tank in the presence of solid particle experimentally. The k_La correlations as a function of propeller rotation speed and flow rate of gas feed were studied. The O_2 and CO_2 absorption in water and in solid-liquid suspensions and heterogeneous precipitation of $MgCO_3$ were thoroughly examined. The absorption experiments of oxygen were conducted in various systems like pure water and in aqueous suspensions of quartz and calcium carbonate particles. Secondly, the precipitation kinetics of magnesium carbonate was also investigated. The experiments were performed to study the reactive crystallization with magnesium hydroxide slurry and carbon dioxide gas by varying the feed rates of carbon dioxide and rotation speeds of mixer. The results of absorption and precipitation are evaluated by titration, total carbon (TC analysis), and ionic chromatrography (IC).

For calcium carbonate, the particle concentration was varied from 17.4 g to 2382 g with two size fractions: 5 µm and 45-63 µm sieves. The k_La and P/V values of 17.4 g $CaCO_3$ with particle size of 5µm and 45-63 µm were 0.016 s^{-1} and 2400 W/m^3. At 69.9 g concentration of $CaCO_3$, the achieved k_La is 0.014 s^{-1} with particle size of 5 µm and 0.017 s^{-1} with particle size of 45 to 63 µm. Further increase in concentration of calcium carbonate, i.e. 870g and 2382g , does not affect volumetric mass transfer coeffienct of oxygen. It could be concluded from absorption results that maximum value of k_La is 0.016 s^{-1}. Also particle size and concentration does affect the transfer rate to some extend. For precipitation experiments, the constant concentration of $Mg(OH)_2$ was 100 g and the rotation speed varied from 560 to 750 rpm, whereas the used feed rates of CO_2 were 1 and 9 L/min. At 560 rpm and feed rate of CO_2 is 1 L/min, the maximum value of Mg ion and TC were 0.25 mol/litre and 0.12 mol/litre with the residence time of 40 min. When flow rate of CO_2 increased to 9 L/min with same 560 rpm, the achieved value of Mg and TC were 0.3 mol/litre and 0.12 mol/L with shorter residence time of 30 min. It is concluded that feed rate of CO_2 is dominant in precipitation experiments and it has a key role in dissociation and reaction of magnesium hydroxide in precipitation of magnesium carbonate.

Table of Contents

Table of Figures

List of Tables

Symbols	Abbreviations	Units
k_g	Total resistance of gas film	kmol/(m^ss)
$1/k_G'$	Liquid film resistance	kmol/(m^ss)
k_G'	Liquid phase mass transfer coefficient	m/s
K_G	Total gas phase mass transfer coefficient	m/s
P^*	Equilibrium partial pressure	kg/(ms)
P	Operational partial pressure	kg/(ms)
E	Enhancement factor	
Δg	Change in free energy per unit molecule	J/mol
Ω	Volume per molecule	
A	Interfacial free energy	J/m^2
r_c	Critical radius	m
ΔG_D	Change in activating free energy	kJ/mol
ΔG_V	Difference in free energies of liquid and crystals per volume of	J/mol
c	Shape factor	
r_*	Radius of spherical nucleus	m
V_m	Molar volume	m^3/mol
H_m	Melting heat	kJ/kg
T_m	Temperature of melting heat of crystal	K
C_p	Heat capacities of liquid and crystal states	J/K
τ	Time needed to established the nucleation	s
ΔH_V	Melting enthalpy of crystal per unit volume	J
k_B	Boltzman constant	J/K

σ_{cm}	Specific free energy	J/mol
N_v	Super-critical nuclei per volume	$1/m^3$
t_{ind}	Induction time	s
φ(r,s)	Agglomeration kernel	
n(r,t)	Particle density	m/m^3
R(s)	Removal rate of particle	m^3/s
S(r,t)	Source rate of particle size	
$\phi_B(r_i, r_j)$	Brownian agglomeration kernel	
T_g	Temperature of continuous phase	K
C_n	Slip factor	
β_c	Collision factor	
β_a	Aerodynamic shape factor	
ϕ_G	kernel of gravitational agglomeration	
y_c	Initial particle separation	
ε_s	Dimensionless sticking of particle	
χ_c	Dimensionless shape factor	
D_H	Hydraulic diameter	m
Re	Reynolds number	
H	Plank's constant	J s
S	Supersaturation	
Ksp	Solubility product	mol/L
A	Ionic Activity	
C_{eq}	Equilibrium concentration	mol/L
R	Gas constant	J/mol K

σ	Surface Energy	J/m^2
Me^+	Concentrations of cation	[+]
X^-	Concentrations of anion	[-]
dc/dt	Change is the crystallization rate	
c_0	Initial concentration	mol/L
A	Area of membrane	m^2
Q	Flow rate	kg/s

1. Introduction

The capturing of CO_2, which is produced by fossil fuel usage, is one of the problematic issues of industries. As we know, CO_2 is major greenhouse gas and it is a source causing global warming and climate change. The major industries for instance electricity generation produces 25% of CO_2 emissions [1]. Furthermore, these emissions are expected to increase by 2.1% per annum [2]. The removal or separation of CO_2 is achieved by numerous methods. The techniques involve physical absorption, chemical absorption, solvent extraction, membrane technology, biological system, cryogenic method and gaseous combustion [3]. The most practical technique for CO_2 capturing from flue gases are mainly chemical solvent methods, which are considered as low-cost and low-energy requirement system. In amine-based system, the CO_2 absorption is based on ionic liquids. The researchers have studied monoethanolamine (MEA) process intensively and succeeded in using this technique commercially for CO_2 recovery.

In this research work, the aim is to investigate the volumetric mass transfer coefficient [k_La] of oxygen in stirred tank in the presence of solid particle experimentally. The k_La correlations as a function of propeller rotation speed and flow rate of gas feed are reported in the articles [4]. In this work, absorption of oxygen as a function of physical parameters are to be focused in various systems, like pure water and suspensions of quartz and calcium carbonate. Secondly, the precipitation process of magnesium carbonate is to be investigated based absorption of CO_2 and the dissolution kinetics study with initially solid reactant, magnesium hydroxide particles. The dissolution rate of magnesium hydroxide in pure water with different feed rates of carbon dioxide gas and rotation speeds of mixer are to be investigated. In order to obtain the concentration of precipition products. This evalution involves titration, total carbon (TC analysis), and ionic chromatrography (IC).

The aim of the present work is to gain deeper understanding on the heterogeneous reactive crystallization with CO_2.

2. Fundamentals of Reactive Crystallization with Gas and Solid Reactant Systems

During the reactive crystallization, reactant solution is mixed with another solution and due to the chemical reactions, the crystallizing substance is produced which increases the solubility. However, the chemical reaction might be adequate or fast, which is highly dependent on mixing conditions and impact the product size distribution. The behavior is different from batch to continuous system. In batch experiment the stirred vessel is used in such away that the whole volume of reactant solutions is mixed promptly. In a continuous process the solutions are fed into the system, however the removal of product could be continuous or semi-continuous. In a semi-batch process, the reactant solution is fed to stirred solution of other reactant, also there is no outlet.

2.1. Absorption of CO_2 in Water

2.1.1. Physical Absorption

In physical absorption, the carbon dioxide [5] absorption into water is done by no chemical reactions. The rate of physical absorption R_0 is determined by film model, which is expressed as:

$$R_0 = \frac{D}{\delta}\,(C^* - C_0) \qquad [6]$$

Here D is the carbon dioxide diffusivity in water and δ is the thickness of stagnant film. The C^* is the concentration of CO_2 at the surface and C_0 is the bulk concentration of CO_2. The equation could also be modified as:

$$R_o = K\sqrt{\frac{D}{t}}\,(C^* - C_0) \qquad [5]$$

Here t is the time and K is the model constant.[7]

2.1.2. Chemical Absorption

Chemical absorption is influenced by the chemical reactions. During the mass transfer process between gas and liquid phases, the total resistance is showed below by the sum of gas film [$1/k_g$] and liquid film resistance [$1/k_G'$]:

$$\frac{1}{k_g} + \frac{1}{k'_G} = \frac{1}{K_G} \quad (3)$$

The total gas phase mass transfer coefficient, K_G, is calculated by:

$$K_G = \frac{Flux}{P_{CO2} - P^*_{CO2}} \quad (4)$$

Here P_{CO2}^* is the equilibrium partial pressure and P_{CO2} is the operational partial pressure of CO_2 in the wetted wall column. P_{CO2} could also be calculated by:

$$P_{CO2} = \frac{P_{CO2,in} - P_{CO2,out}}{Ln\left(\frac{P_{CO2,in}}{P_{CO2,out}}\right)} \quad (5)$$

The liquid phase mass transfer coefficient i.e. $k_{G'}$ is calculated by:

$$k'_G = \frac{Flux}{(P_{CO2,i} - P^*_{CO2})} \quad (6)$$

The partial pressure of CO_2 at the gas liquid interface, i.e. $P_{CO2,i}$ is calculated by:

$$P_{CO2,i} = P_{CO2} - \frac{Flux}{k_g} \quad (7)$$

The $k_G^{'}$ can also be expressed as:

$$\frac{1}{k'_G} = \frac{H}{k_l^0\ E} \quad (8)$$

Here 'E' is the enhancement factor which is defined as the ratio of flux with chemical reactions to without chemical reactions [8].

2.2. Nucleation

When the free energy of previous phase becomes higher compared to new phase, the development of new phase from previous phase, is known as nucleation. (Hohenberg and Halperin 1977; Chaikin and Lubensky 1995). The nucleation formation transpires due to the action of tiny nuclei of new phase present inside the bulk volume of previous phase, which is metastable. Metastability is associated with the change in free energy of formatted nucleus. The surface molecules of both phases (new and old) are not tightly bounded in comparison to bulk, which plays integral role in increasing the free energy of

new phase. The interfacial free energy; *difference between the free energy per molecule of the bulk and that of the surface is referred to as the interfacial free energy*, is a key parameter which destabilize the nucleus. Even if more molecules are introduced to increase the free energy, such nucleus will be dissolved instead of growing. On the other hand if the size of nucleus becomes huge enough, the decrease in free energy related with development of the bulk phase becomes significantly high, the surface free energy is irrelevant [9].

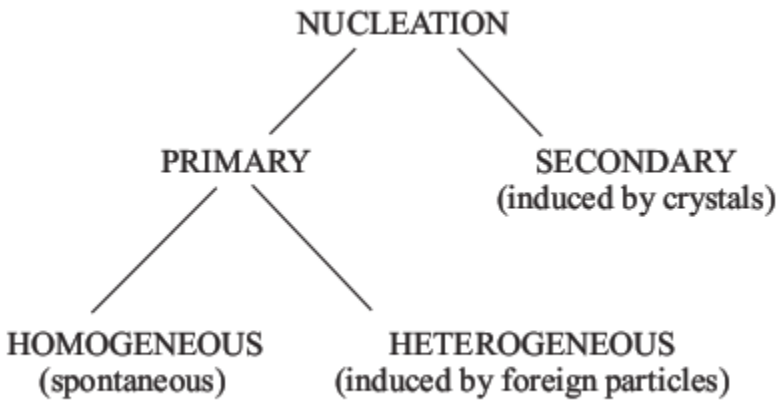

2.2.1. Classical Nucleation

According to Bazant [10] the concept of heterogeneous nucleation is better understandable with the help of geometry system. For instance, spherical nucleus with radius '*r*', showed in figure below forms nucleus within the bulk solution. This is considered as homogeneous nucleation.

$$\Delta g = \Delta g_b + \Delta g_s \tag{9}$$

$$\Delta g = -\left\{\frac{\left[\left(\frac{4}{3}\right)\pi r^3\right]}{\Omega}\right\}\Delta\mu + 4\pi r^2\alpha \tag{10}$$

Here Δg is the change in free energy per unit molecule, Δg_b is the change in free energy of the bulk and Δg_s is the surface term. The Ω is the volume per molecule and α is interfacial free energy.

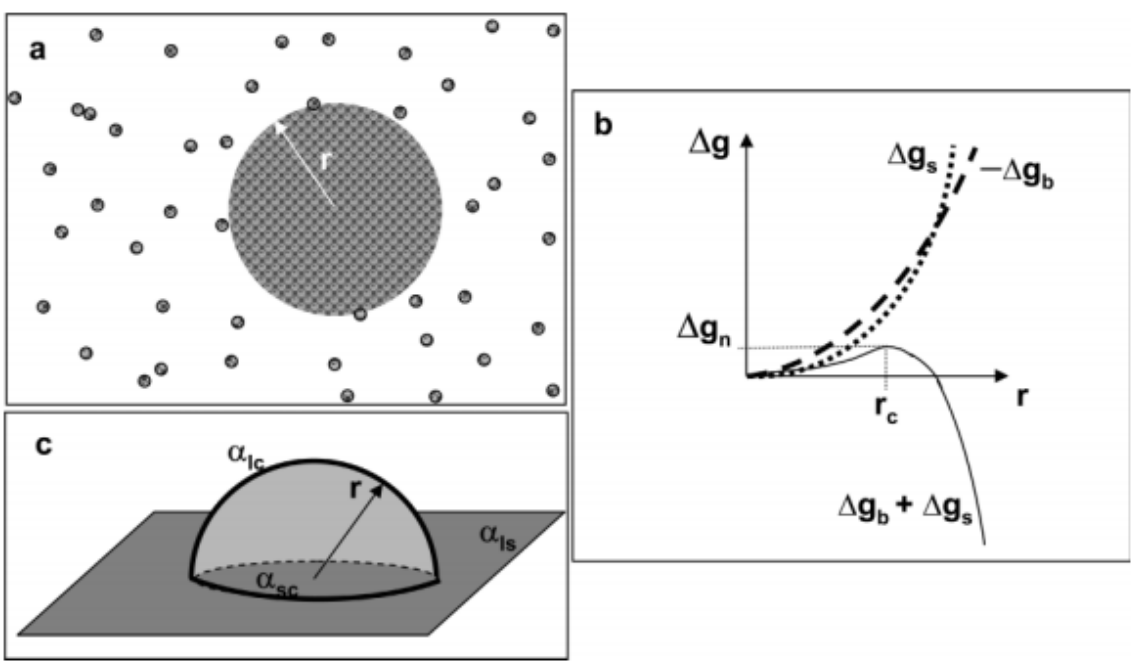

Figure 1 (a) The spherical nucleus with radius 'r' is showed (b) The bulk and other surface are combined and they tend to have barrier of free energy (c) The hemisphere nucleus of heterogeneous nucleation on foreign particle [10].

$$r_c = 2\Omega\alpha/\Delta\mu \tag{11}$$

$$= \frac{2\Omega\alpha}{kT\sigma}$$

In heterogeneous nucleation, there are two interfacial energies; firstly it is between crystal and the solution and secondly between crystal and the particle. Assuming the nucleus as hemisphere of radius r, for heterogeneous nucleation, the above equation is manipulated as:

$$\Delta g = -\left\{\frac{\left[\left(\frac{2}{3}\right)\pi r^3\right]}{\Omega}\right\}\Delta\mu + \pi r^2(\alpha_{lc} + \alpha_{sc} + \alpha_{ls}) \tag{12}$$

The lc,ls and sc are liquid crystals, liquid solids and substrate crystals and k_B in equation 13 is boltzman constant. The critical radius for heterogeneous nucleation is:

$$r_c = \frac{2\Omega\alpha'}{k_B T\sigma} \tag{13}$$

where

$$\alpha' = \alpha_{lc}\left\{1 - \frac{(\alpha_{ls} - \alpha_{sc})}{2\alpha_{lc}}\right\} \tag{14}$$

2.2.2. Homogeneous Nucleation

According to Schmelzer [11] in homogeneous nucleation, the formation of critical nucleus in given surface or volume follows the classical nucleation theory (CNT). The nucleation rate of steady state homogeneous volume is written as:

$$I_{st} = I_0 \exp\left[-\frac{W_* + \Delta G_D}{k_B T}\right] \tag{15}$$

where

$$I_0 = 2N_1 \frac{k_B T}{h}\left[-\frac{a^2\sigma_{cm}}{k_B T}\right]^{1/2} \tag{16}$$

The above expression determines number of supercritical clusters per unit time in unit a given volume. The term I_0 depends upon temperature and its value changes from 10^{41} to 10^{43} m^{-3} s^{-1}. Here k_B and h are Boltzmann and planck constant, σ_{cm} is specific free energy, and ΔG_D is change in activating free energy. The critical nucleus size is determined by:

$$\frac{\delta W}{\delta r} = 0 \tag{17}$$

$$W = c_1 r^2 \sigma_{cm} - c_2 r^3 \Delta G_V \tag{18}$$

Here ΔG_V is the difference in free energies of liquid and crystals per volume of crystal and shape factor is donated by c_1 and c_2. If the nucleus is spherical, then:

$$r_* = \frac{2\sigma_{cm}}{\Delta G_V} \tag{19}$$

$$W_* = \frac{16\pi}{3} \frac{\sigma_{cm}^3}{\Delta G_V^2} \tag{20}$$

The driving force can be written as:

$$\Delta G_V V_m = \frac{\Delta H_m}{\Delta T_m}(\Delta T_m - T) + \int_T^{Tm} \Delta C_p dT' - T \int_T^{Tm} \frac{\Delta C_p}{T'} dT' \tag{21}$$

The term V_m is molar volume, ΔH_m and ΔT_m are melting heat and temperature of melting heat of crystal in moles and ΔC_p is change in heat capacities of liquid and crystal states.

$$\Delta G_V(T) = \Delta H_V \left(1 - \frac{T}{T_m}\right), \Delta G_V(T) = \Delta H_V (1 - \frac{T}{T_m}) \frac{T}{T_m}, \tag{22}$$

Where ΔH_V is the melting enthalpy of crystal per unit volume. The time needed to established the nucleation is donated by 'τ', the expression is as follows:

$$\tau = \frac{16h}{\pi} \frac{\sigma_{cm}}{\Delta G_V^2 a^4} exp\left(\frac{\Delta G_D}{k_B T}\right) \tag{23}$$

$$I(t) = I_{st}[1 + 2\sum_{m=1}^{\infty}(-1)^m \exp\left[-\frac{m^2 t}{\tau}\right] \tag{24}$$

After integrating the equation, the time dependency of super-critical nuclei per volume N_v is given as:

$$\frac{N_V(t)}{I_{st}\tau} = [\frac{t}{\tau} - \frac{\pi^2}{6} - 2\sum_{m=1}^{\infty} \frac{(-1)^m}{m^2} \exp(-m^2 - \frac{t}{\tau})] \tag{25}$$

$$N_V(t) = I_{st}[t - \frac{\pi^2}{6}\tau \; for \; \tau \to \infty \tag{26}$$

In order to estimate experimental τ, it is appropriate to use induction time t_{ind}, which is given as:

$$\tau = \frac{6}{\pi^2} t_{ind} \tag{27}$$

2.2.3. Spinodal Decomposition

The fluctuation of concentration in a system of multiphase fluid is discussed by Gibbs-Thomson theory of homogeneous nucleation. And the boundary between instable and metastable of the bulk phase is called a spinodal line. The critical size has numerous effects for instance in controlling the nucleation because nucleation is highly affected by critical nucleus size value. If the value of interfacial energy is small, the critical size is small too and nucleation will occur during supersaturatin. Consequently, if fluid composition or supersaturation is varied, the nucleation might be influenced [10]. According to Gibb's theory:

$$\left.\frac{\partial^2 G}{\partial c^2}\right|(T,P) = 0 \tag{28}$$

Here 'G' is the free energy per mole of solution and 'c' is fluid concentration as the function of temperature and pressure. In order to spinodal decomposition to occur it is necessary that:

$$\left(\frac{\partial^2 G}{\partial c^2}\right) \leq 0 \tag{29}$$

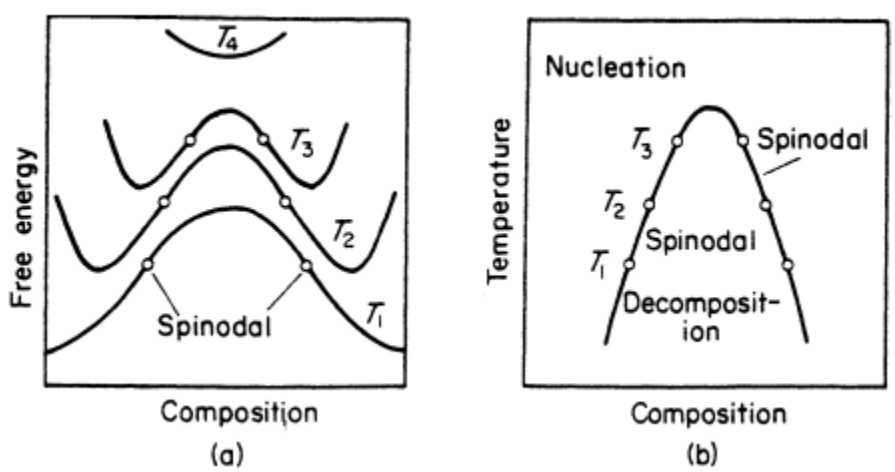

Figure 2 (A) Relationship between free energy and composition(B) and relationship between temperature and composition [10]

2.2.4. Heterogeneous Nucleation

The introduction of foreign particles plays important part in controlling the nucleation. The foreign surface lowers the interfacial energy between the nucleus of crystals and solid substrate is lower as compare to crystal; which is in contact with the solution. The molecules of crystal make bonds with substrate which is stronger as compare to the bonds of solvation.

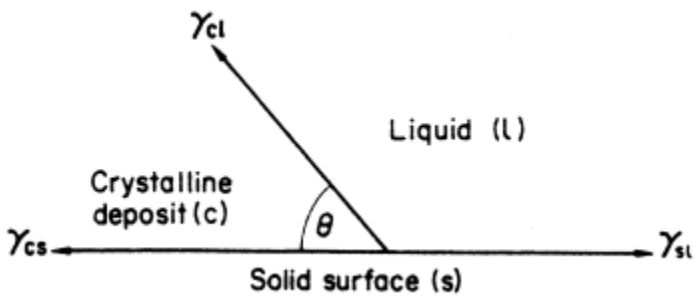

Figure 3 the contact angle and interfacial forces for all multiphase.

The enthalpic of free energy is mainly coming from chemical bond, which is strong and lower the interfacial free energy. It allows delineating the orientation and location of crystal. No dubious that the bond strength is sturdily proportional to structure and chemistry of the foreign particle. If the internal structure of particle body is matched the nucleating phase plane, the lattice strain is minimized, and furthermore it promotes chemical bond to nucleus. That promotion leads to minimize enthalpic contribution for interfacial free energy; therefore the nucleation develops favorably on that crystal plane. Thermodynamically, nucleation could be controlled by varying interfacial energy, by increasing in supersaturation, and changing rate of adsorption or desorption. To quantify the concepts, the precipitation of nucleus size and its dependency on free energy is considered above [12].

2.2.5. Influence of Gas Flow Rate and Mixing Intensity

The nucleation as the function of physical parameters for instance type of concentration of the fluid mixing intensity have been reported in the articles [13-15]. The metastable zone width (MSZW) influences in designing and optimizing the crystallization process, in order to achieve spontaneous nucleation the high mount of supersaturation is needed. Typically, it is desirable to operate away from this metastable limit so as to ensure eliable

process performance. Metastable one information can be used to optimize crystallization processes [16] and calculate nucleation kinetics. The MSZW may be affected by various process parameters, such as supersaturation generation rate [17] and agitation speed [18].

Based upon the literature review, for experimental work, the most common technique to measure the nucleation rate is determined by Focused beam reflectance measurement (FBRM) and attenuated total reflectance-Fourier transform infra-red (ATR-FTIR) spectroscopy. FBRM is a probe-based instrument which detects the shape, size and population density of the system. It could also determine the degree of change and the rate of change for the dynamic system. Furthermore it dominates the off-line techniques because of in situ facility.

Some researchers have used modeling tools like Computational Fluid Dynamics (CFD) to study the impact of mixing on reactive crystallization [6, 19]. Computational fluid dynamics (CFD) software plays important part in vindicating the experimental work. The most common mixing models are volume of fluid (VOF), Eulerian model, mixing model and disperse phase model (DPM). CFD has been used to model batch, semi-batch and continuous reactors for reactive crystallizations and has predicted tremendous result and behavior of the system [20]. It has been used immensely to predict the particle distribution, particle size, product yield, kinetics of crystallization, feed rate, and mixing rate.[21]

The laminar or turbulence fluid flow conditions by mixing could be achieved. In laminar mixing approach the transport and thermodynamic properties of gas is to achieve supersaturated state and precede nucleation. The gas is saturated and containing hot nucleating vapor transfers to condenser section, where the vapor transforms into supersaturation state and makes condensed phase. The newly nucleated particles move from nucleation zone to the supersaturated environment. The nucleation rate is around from 10^2 to 10^8 $cm^{-3}s^{-1}$ in this method. The laminar flow diffusion chamber is not suitable for vapors of low molecular weights for instance water. It lacks the well-defined nucleation zone due to the thermal diffusivity also it is hard to measure rate of nucleation. In case of Turbulent Mixing Chamber; which is mainly for binary or ternary nucleation, it consists of turbulent mixing chamber accompanied by laminar nucleation portion. Multi-

gas flow chambers are holding nucleating vapors which are instantaneously mixed in turbulent flow [22].

2.3. Crystal Growth

In crystal growth, one of the main challenges is to describe and understand the physical mechanisms how crystal growth can be controlled. In general, we could illustrate the "energy landscape," in Figure 2. Energy landscape elucidates that the crystallization is phase transition in which substance is transferred from high free energy to lower free energy in crystal lattice. The shape of landscape determines the crystal properties for instance habit, phase and growth rate. The depths and shapes of energy minima control the phase and the equilibrium crystal habit. Therefore, just by changing the heights of barriers, it is easy to control the intermediate, non-equilibrium and crystal growth kinetics

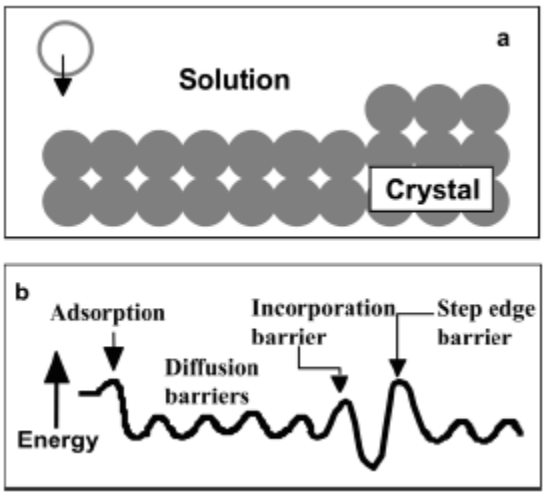

Figure 4 Schematic of (a) The physical landscape and (b) energy landscapes of growing crystal.

Different types of crystals are formed, which are proportional to operating condition and final product. The shapes of crystal are orthophombic, hexagonal, cubic, triclinic, hexagonal, monoclinic, tetragonal, and trigonal. Certain prerequisite must be achieved in order to precede crystal growth, for instance sufficient supersaturation degree. The crystallites grow with particular geometry which is related with collagen fibres and crystal lattice along with an *axis lying by the length of fiber and the axis pointing along the rows of hole zones*. *This implies molecular-scale control by the collagen molecules over both the orientation and location of the crystal nuclei.*

In primary nucleation, usually many nuclei are formed spontaneously which are crushing out of the solution. During continuous crystallization, soon the primary nucleation starts, crystal size distribution initiates to make shape. The other mechanism of crystal growth is done via secondary nucleation, the growth of crystal initiates with contact. This contact could be of solution to pipe, mixer or a vessel wall. On contrary to primary nucleation, the secondary nucleation operates at lower supersaturation and achieves optimal crystal growth. Furthermore in secondary nucleation, the seed or existing crystals impact secondary nucleation mechanism. Unfortunately the complete theory to model secondary nucleation is not available and therefore the behavior can only be examined by experiments. Mathematic relationships do exist to correlate experimental data. Some correlated experimental data is available, however it is often time consuming to model crystallization for batch operations unlike continuous process [11, 12]. The basic thermodynamics of crystal growth is given by Gibbs Thomson, the change in the free energy and change in chemical potential are proportional to activity products 'AP', which are described as:

$$aA + bB + \cdots . + nN \rightarrow A_a B_b \ldots \ldots Nn \tag{30}$$

$$AP = [A]^a\ [B]^b\ [C]^c \ldots \ldots [N]^n \tag{31}$$

$$K_{sp} = [A]_e^a [B]_e^b [C]_e^c \ldots \ldots [N]_e^n \tag{32}$$

$$\Delta g_{sol} = -k_B T ln K_{sp} \tag{33}$$

$$\Delta\mu = k_B T \ln\sigma \tag{34}$$

$$\sigma = \ln(\frac{AP}{K_{sp}}) \tag{35}$$

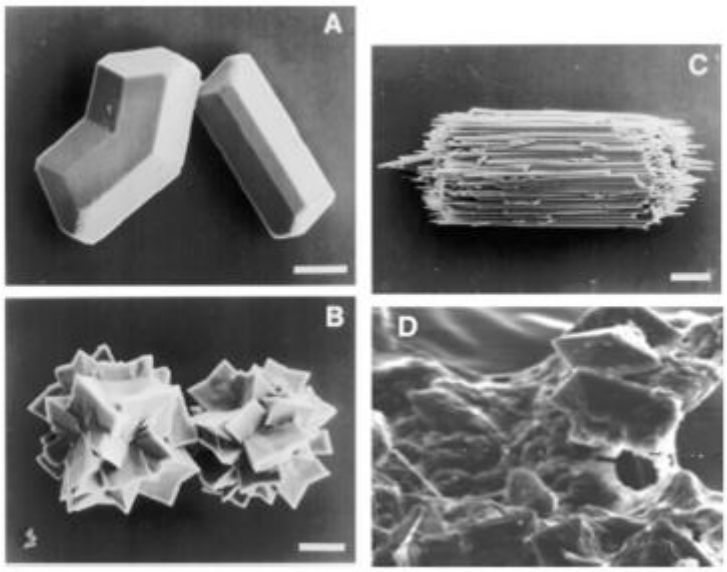

Figure 5 The different types of crystal (a) twinned/prismatic crystal (b) Druse crystal (c) Isolated bundle of needle crystal (d) crystal growth on unretal stent [10]

2.4. Agglomeration

Agglomeration is not phenomenon just like nucleation and growth, which occurs during all crystallization process. It is highly dependent upon physical and operating conditions of the process. Normally agglomeration happens due to sticking behavior of crystal with each other and makes large size crystals than normal ones. The agglomeration process has three types[23]:

- Based upon cohesion force, which is weak and resulted product is called coagulation or flocculation.

-If supersaturation sticks crystals hardly along with crystal growth of mother particles is called agglomeration.

In order to achieve agglomeration, it is necessary that two particles must collide with each other and certain residence time must be given for the particles to hold each other. Also the adherence is required which is caused by supersaturation. The forces that bonds the crystal works as a bridge, and the forces are weak for instance van der Waals forces. The agglomeration is highly dependent upon operation conditions of crystallization as mentioned above. Therefore the most important parameters are mixing, small/large eddies of turbulent flow, viscosity and density of fluid, the required particle size, residence time in vessel, population density of crystal, nucleation and growth and impurities in the solution.

In flocculate the particles sticks with another primary particle by the action of cohesive forces which are also weak. Aggregation is intermediate process of agglomeration and flocculation with or without supersaturation. Both flocculates and aggregates could be formed with and without supersaturation and they are easily demolished. On the other side, agglomerates occur in supersaturated solutions only[24, 25].

There are two major types of crystal agglomeration primary and secondary agglomeration. The primary agglomeration is result of polycrystals, twins and dentrites whereas secondary agglomeration happens in supersaturation state due to crystal-crystal collision. The secondary agglomeration normally occur in suspended particle solution, the factors that influence this system, are mechanical process, fluid dynamic, kinetic of

crystallization, and particle behavior. Agglomeration dominates the system with particle size less than 50 µm, beyond this limit agglomeration is not affected. The critical size is important in agglomeration and certain limit of critical size must be obtained; the critical size proportional to crystal growth, power input and suspension density.

The agglomeration starts after formation of small primary particles in primary nucleation. Initially, in supersaturated solution the rate of homogeneous or heterogeneous primary nucleation governs the number of particles. During induction period the agglomeration is negligible for a curtain short period of time i.e. few seconds. But after couple of minutes agglomeration starts and literature confirms that agglomeration is accomplished when the particle size has reached 10–30 micro meters [23].

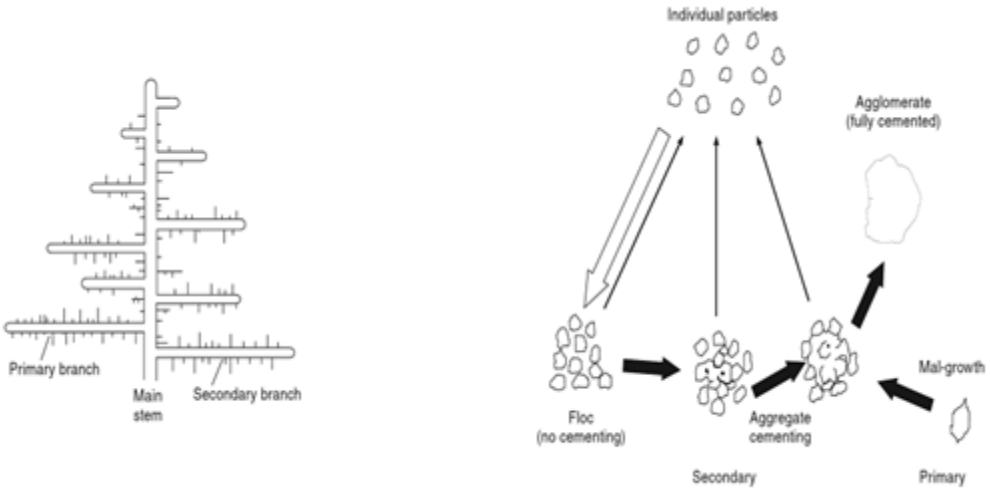

Figure 6 Left hand side shows typical structure of dendrites and right hand side the formation of aggregation and agglomeration[26].

2.4.1. Spherical Agglomeration

During the spherical agglomeration,the agglomeration and spheronization occur simultaneously in a single step and the end product is called spherical agglomerate. During this process the formation crystals aggregates are joined together by liquid bridges; these bridges are made by external agitation of crystals in liquid suspension, also the binding agent is present in that solution. The immiscible binding agent has tendency to hold the particles to be agglomerated.

The example of drugs like paracetamol could be taken into account as a controlled utilization of agglomeration. This drug is in solid form is hard to make it into tablet shape via direct compression. Therefore agglomeration solves this problem by making even distribution of agglomerates. These types of agglomerates are formed by sinking out the paracetamol drug from mixture of tricholoromethane and hexane accompanied by binding agent i.e. water. The immiscible water wets the drug and forms thin film on the surface, whereas the hardness is achieved by solid bridges. Furthermore the binding agent could also act as reversible agglomeration in order to improve filtration of tiny particles; which are hard to filter compared to larger particles. The resulted binding agent is being evaporated during drying process [27, 28].

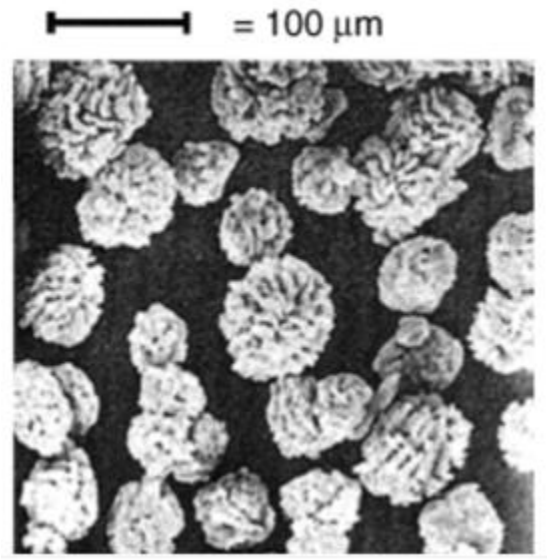

Figure 7 Spherical agglomerates of paracetamol is accomplished by the action of controlled crystallization.

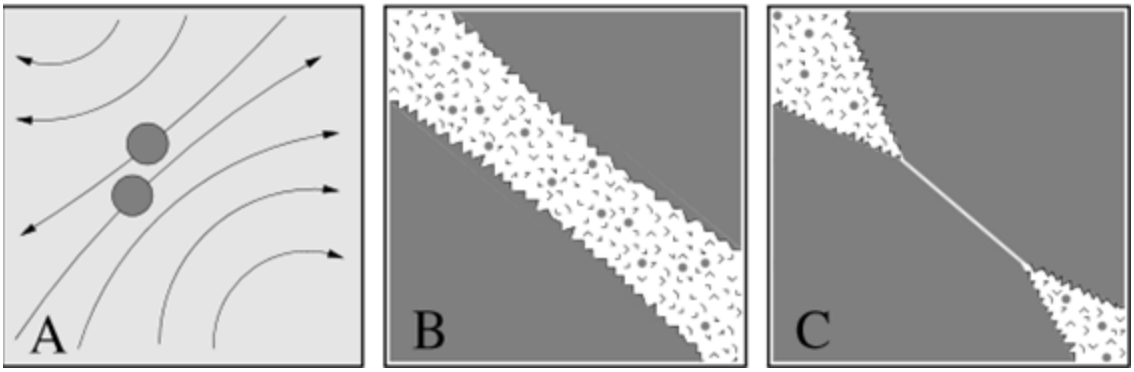

Figure 8 The agglomeration of crystal in stages are mentioned here, (A) Two crystallites are approaching with each other to collide (B) for nanometers distance and contact the solute and solvent to determine interaction of crystallites, (C) after interaction of both crystalites, the link (bridge) is created between them which is dependent upon crystal growth rate and supersaturation.

2.4.2. Agglomeration Mechanism

The agglomeration mechanism includes brownian agglomeration, gravitational agglomeration, turbulent agglomeration and electrostatic agglomeration; these mechanisms are mass conserving. This phenomenon lowers the diffusibility and tends to settle down quickly due to gravitational forces. Also agglomeration decreases surface area of particles, which is not appreciated in some cases for instance chemical reactions. The rate equation is used to determine particle size distribution, which is:

$$\frac{\partial}{\partial t} n(r,t) = \frac{1}{2}\int_0^r \phi(s, r-s) n(s,t) n(r-s,t) ds - n(r,t)\int_0^\infty \phi(r,s) n(s,t) ds - n(r,t) R(r) + S(r,t) \tag{36}$$

Here φ(r,s) is the agglomeration kernel, n(r,t)dr is the particle density, R(s) is the removal rate of particle and S(r,t) is the source rate of particle size [29].

2.4.2.1. Brownian Agglomeration

Brownian motion is studied by Robert Brown. It is a study of continuous random movement or diffusibility of suspended particles in a fluid. In agglomeration the particle collide and join with other particles in a random way, therefore Brownian agglomeration

plays important role. Initially Smoluchowski calculated the Brownian agglomeration in 1916. According to Smoluchowski:

$$\phi_B(r_i, r_j) = 4\pi k_B T_g \beta_c \left[\left(\frac{C_n r_i}{6\pi\mu r_i \beta_a}\right) + \left(\frac{C_n r_i}{6\pi\mu r_i \beta_a}\right)(r_i + r_j)\right] \quad (37)$$

Here $\phi_B(r_i, r_j)$ is the Brownian agglomeration kernel; which is called Perkins, , T_g the temperature of continuous phase, C_n the slip factor (Cunningham), β_c the collision shape factor, the dynamic viscosity and aerodynamic shape factor are denoted by μ and β_a.

2.4.2.2. Gravitational Agglomeration

The gravitational agglomeration happens due to size dependence of tiny particles terminal velocity. The smaller particle settlement is apprehended by rapid settlement of larger particles. The kernel of gravitational agglomeration ϕ_G is mentioned as:

$$\phi_G(r_1, r_2) = \pi y_c^2(r_1, r_2)\left|v_s(r_1) - v_s(r_2)\right| = \pi(r_1 + r_2)^2 \varepsilon_G(r_1, r_2)\left|v_s(r_1) - v_s(r_2)\right| \quad (38)$$

Here y_c is the initial particle separation and v_s (r) the particle settling velocity. The collision efficiency of gravitational agglomeration is given as:

$$\varepsilon_G(r_1, r_2) = \frac{y_c^2}{(r_1 + r_2)^2} \quad (39)$$

The tiny particles tend to have negligible effect as compared to larger particles. Based upon Fuchs assumption, the collision efficiency of gravitational agglomeration is written as:

$$\varepsilon_G = \frac{3(r_1/r_2)^2}{2(1 + (r_1/r_2))^2}. \quad (40)$$

The Pruppacher and Klett (1978) added the velocities of particle, the above equation is modified as:

$$\varepsilon_G = \begin{cases} \dfrac{(r_1/r_2)^2}{2(1+(r_1/r_2))^2}, & r_1/r_2 \le 0.46 \\ 0.05, & 0.46 < r_1/r_2 \le 1 \end{cases} \tag{41}$$

Above equations does not consider absolute particle size, therefore Pertmer and Loyalka presented the momentum equation, which is absolute particle size dependent as:

$$\frac{4}{3}\pi\rho_i r_i^3 \frac{d\underline{u}_i}{dt} = \frac{4}{3}\pi(\rho_i - \rho_f) r_i^3 \underline{g} - \underline{F}_i, \tag{42}$$

2.4.2.3. Turbulent Agglomeration

The turbulent agglomeration is divided into shear and inertial turbulent agglomeration. The turbulent shear agglomeration deals with particles which are following the flow pathlines and collide with each other. This behavior is obvious because every particle is on different streamlines and hence moving with various speeds; as a result turbulent shear agglomeration happens. According to Saffman and Turner model, the rate of agglomeration ϕ_s is given as:

$$\phi_s(r_1, r_2) = \varepsilon_s \varepsilon_{PK}(r_1, r_2) \chi_c^{\,3} [r_1 + r_2]^3 \sqrt{\frac{8\rho_f \pi \phi_T}{15\mu}} \tag{43}$$

Here ε_s is the dimentionless sticking of particle to particle efficiency, ε_{PK} the dimensionless correction factor of collision, χ_C the dimensionless shape factor of collision, ρ_f the density of fluid, μ the dynamic viscosity and ϕ_T the dissipation rate. The turbulent energy dissipation rate is elucidated as:

$$\phi_T = \frac{0.03146 U^3}{D_H \, \mathrm{Re}^{3/8}} \tag{44}$$

The speed of fluid is denoted by U, the hydraulic diameter D_H and Reynolds number Re. The agglomeration kernel ϕ_I is given as:

$$\phi_I(r_1, r_2) = \varepsilon_s \varepsilon_{PK}(r_1, r_2) \chi_c^{\,2} [r_1 + r_2]^2 \left(\frac{512 \rho_f \pi^3 \phi_T^{\,3}}{15\mu} \right)^{1/4} \frac{[v_s(r_1) - v_s(r_2)]}{g} \tag{45}$$

This turbulent model has some difficulties and in some cases it is hard to apply on agglomeration processes. Also the presented model of Saffman and Turner is in developing stage, hence it is unvalidated. The agglomeration process in turbulent flows has vital importance especially when dealing with higher dissipation rates of energy [29].

2.4.2.4. Electrostatic Agglomeration (DLVO THEORY)

The DLVO theory is developed by Derjaguin and Landau. This mathematical theory includes two major forces dominating in system. The forces are van der Waals and electrostatic repulsion forces. Beside attraction force, the Van Der Waals force also contains repulsion due to the act of overlapping and attraction are Keesom,London and Debeye forces[29] . The Keesom force of attraction implies between dipolar molecules. The Debeye force are also force of attraction which is between stable dipole molecules and induced dipole molecules. Lastly, the London forces are for non-polar molecules due to the instantaneous fluctuation in charge distribution near surrounding of molecules. The interaction of two dipoles is calculated by:

$$E_k(D) = -\frac{u_1^2 u_2^2}{3(4\pi e_0 e_r)^2 KTD^6} \tag{46}$$

The dipole moment is represented by 1 and 2 in molecules, ‘e’ and ‘er’ is the electric field constant and permittivity. The distance between molecules is denoted by D. The Debeye force of attraction is mentioned as:

$$E_D(D) = -\frac{(u_1^2\alpha_2 + u_2^2\alpha_1)}{3(4\pi e_0 e_r)^2 KTD^6} \tag{47}$$

The mathematical equation for London forces of attraction is given below, here planck’s constant is denoted by ‘h’ and frequency is represented by ‘v’.

$$E_L = -\frac{3\alpha_0^2 hv}{(4\pi e_0)^2 D^6} \tag{48}$$

Futhermore, it is important to understand the interparticle potentials in order to determine the nature of agglomeration and their kinetics. In case of diffusion limited aggregation process, the potential energy barrier to from agglomeration is zero. The primary particle

collide with other particle and tends to stick; the newly formed agglomerate is open in structure with lower fractional dimension. If there is energy barrier for instance reaction process, the particles will stick to those regions where the potential energy sites is lower and tends to agglomerate densely at higher fractional dimensions [30, 31].

3. Precipitation of Calcium and Magnesium Carbonates

The precipitation of a solute from homogeneous solution is occuring by transformation of liquid phase into solid phase. The precipitation is also referred as fast crystallization because the high rate of crystallization is related to high supersaturation stage. Therefore, precipitation starts at high supersaturation level. There are different processes involved in precipitation, which are showed below in figure 9. The precipitation starts in supersaturation solution of homogeneous or heterogeneous nucleation. We know that nucleation is considered as difficult step, in order to initiate the precipation; the energy barrier needs to be overcome. This energy barrier is connected with change in Gibbs energy of nuclei. The nuclei is created either by embryos and homogeneous nuclei or by means of foreign solid phase, which may be present already in heteronuclei. Normally nuclei dimensions less than 100 growth units are neglected. The crystal growth playes significant role in concentration of precipitating phase. Theoratically, the termination of precipitation process happens when crystals form equilibrium with saturated solution. However practically, precipitation is accomplished with certain crystal size which may cause sedimentation [32].

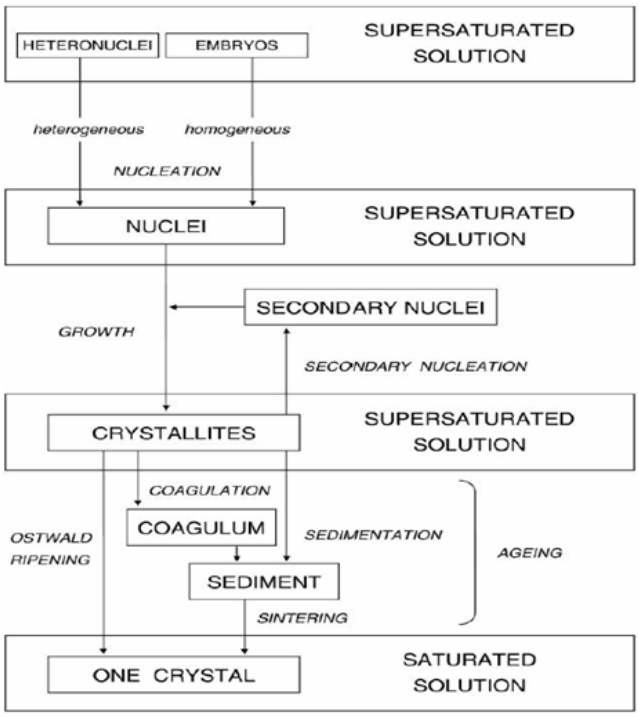

Figure 9 Steps involved in precipitation process.

The ageing occurs at equilibrium and has multiple options. In early steps of precipitation, the Ostwald ripening and recrystallization are most likely to take place. The coagulation and agglomeration process are occurred in sintering . In case of metastable phases of amorphous solids, hydrates and polymorphs, they have numerous stability and solubity behavior based upon thermodynamics. This phenomenon was reported by Ostwald. According to Ostwald, the unstable phase (or least stable) has higher solubility and consequently it precipitates firstly and makes stable phase.

The physico-chemical properties of produced inorganic solid precipation from solution depends on various factors. The major factors in precipitation process are mechanisms of nucleation, crystal growth and ageing. These factors could be confined by selecting appropriate precipitation model and experimental conditions, eventually there is a possibility of acceptable behavior of produced precipitated solute [33, 34].

3.1. Physical and Thermodynamic Properties

3.1.1. Energy Driving Force of Supersaturation and Solubility

The supersaturation is the main parameter in precipitation process which controls nucleation, Ostwald ripening and growth rate. The sparingly soluble precipitation is normally reached when reacting species are being mixed. It is important to know the solubility of precipated product to estimate the driving force in precipitation. In the case of coexisting equilibrium of precipitate, the supersaturation (*S*) is defined as:

$$S = \frac{\pi}{K_{sp}} = \frac{a_A a_B}{K_{sp}} \tag{49}$$

Here K_{sp} is the solubility product and a is the ionic activity of species. The supersaturation could also be expressed as:

$$S = (\frac{\pi}{K_{sp}})^{\frac{1}{v}} = (\frac{a_A^{v+} a_B^{v-}}{K_{sp}})^{\frac{1}{v}}, v = v^+ + v^- \tag{50}$$

Here number of moles of ions is denoted by v, in case of concentration:

$$S = \frac{C}{C_{eq}} \tag{51}$$

C_{eq} is equilibrium concentration at solubility, the driving force of supersaturation is difference in concentration.

$$\Delta C = C - C_{eq} \tag{52}$$

3.1.2. The Equation of Gibbs-Thomson and Surface

The equation of Gibbs-Thomson is related with the size of crystal accompined by solubility equilibrium. The solubility equilibrium of for instance spherical crystal is given as:

$$ln\frac{C_{eq}(r)}{C_{eq}(\infty)} = \frac{2\sigma V_m}{RTr} \tag{53}$$

Here r is the radius of crystal related with ∞ which is the very large size crystal, σ the surface energy, Vm the volume of molecules and R the gas constant. Based upon Gibbs-Thomson equation, the surface energy of precipitated substance is not well fitted with experimental data. Later on Sohnel and Garside determined the value of surface energy as a function of the solubility, which is around eight orders of magnitude approximately. This equation of Gibbs-Thomson is still important for sparingly soluble precipites.

3.1.3. Precipation Diagram (PD)

The precipation diagram is of prime concern in which precipate is formed from reactions. Therefore, the conditions of reaction could be figured out from the diagram shown below. The precipitation diagram for sparingly soluble precipitate represents concentration, temperature, pH and other relavent properties. Let us consider idealized PD in below mentioned coordinates, the $[Me^+]$ and $[X^-]$ are concentrations of cation and anion. The equivalence line is the straight line, which is bisecting the diagram.

$$p[Me^+] = -\log[Me^+] \ verses \ p[X^-] = -\log[X^-] \tag{54}$$

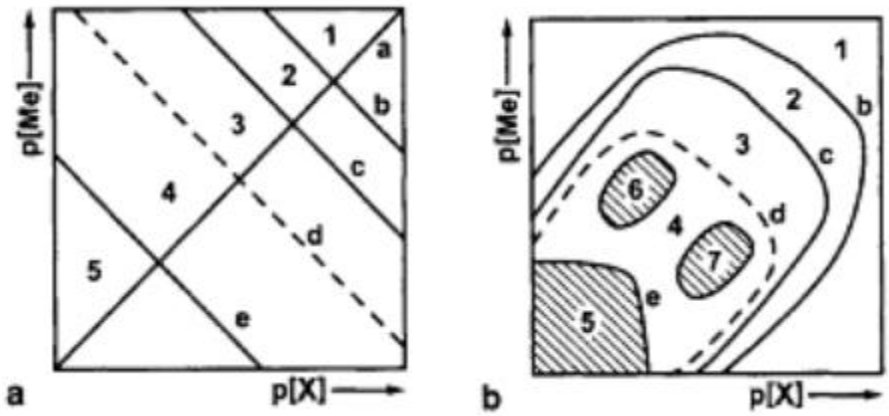

Figure 10 (A)Ideal precipitation and (B) diagram of non-linear precipitation.

If the precipitation is not following stoichiometric reactions, but on the other hand forms polymeric components which are transfored from one another at different rates; the total anion concentration is elucidated as [35]:

$$[X] = [X^-] + [MeX] + [MeX_2^-] + \cdots \tag{55}$$

The precipitation of calcium carbonate occurs around 325 to 460 ppm at alkaline pH with saturation index of 0.5 to 1.1. The precipipitation of calcium carbonate is done in the absence of seed crystals or in the presence of seed crystals. In the absence of seed crystals, although the saturation index (S.I) is positive, the precipitation does not occur unless adequate supersaturation is achieved. This supersaturation will stabilize the nuclei as activation energy barriers are not exceeded. The activation energy is proportional to relative saturation or supersaturation.

$$DG_a = \frac{16\pi\sigma^5 v^2}{[3(kTlnS)^2]} = \frac{B}{(SI)^2} \tag{56}$$

The rate of nucleation of nuclei as a function of activation energy is given as:

$$J = A\exp\left(\frac{-\Delta G}{kT}\right) = Aexp[-\frac{C}{(SI)^2}] \tag{57}$$

Here *A* is the efficiency constant of collisions between calcium and carbonate ions and *C* the constant as well. As it is mentioned above that activation energy DGa is proportional to SI, therefore higher the saturation index, the activation energy barrier will be low, and hence the rate of nucleation will be higher.

In the presence of seed crystals, the rate of precipitation of calcium carbonate in supersaturated solution is repsesented by differential equation as:

$$\frac{dc}{dt} = -ks(c - c_0)^2 \quad (58)$$

Here dc/dt change is the crystallization rate, k the rate constant, s the surface area of crystals, c_0 the initial concentration and c the final concentration of calcium carbonate [36, 37].

4. $C0_2$ Recovery from Flue Gases

It is practically observed that the CO_2 recovery from flue gas is different compared to other gas treatment plant. For instance, in natural gas, gas sweetening and ammonia plant partial pressure of CO_2 is relatively low. Furthermore CO_2 recovery plants are mostly sensitive to SOx and NOx [38]. In case of coal-fired boilers which contain SOx, soot, and fly ash, the CO_2 recovery plant must also deal with it. The CO_2 partial pressure is near to ambient pressure with concentration between 3 to 15%. Concentration of any gas plays integral role in cost analysis, based upon the second law of thermodynamics (entropy) that the mimimum energy requirement to separate higher concentration of CO_2 is less than lower concentration of CO_2 in flue gas, showed below in Figure 11. As we know that most of the gas treatment processes are operating at higher pressure and in order to use these processes the pressures are needed to be normalized via compressor. The cost of compressor is high and as the result the process is not economically satisfactory.

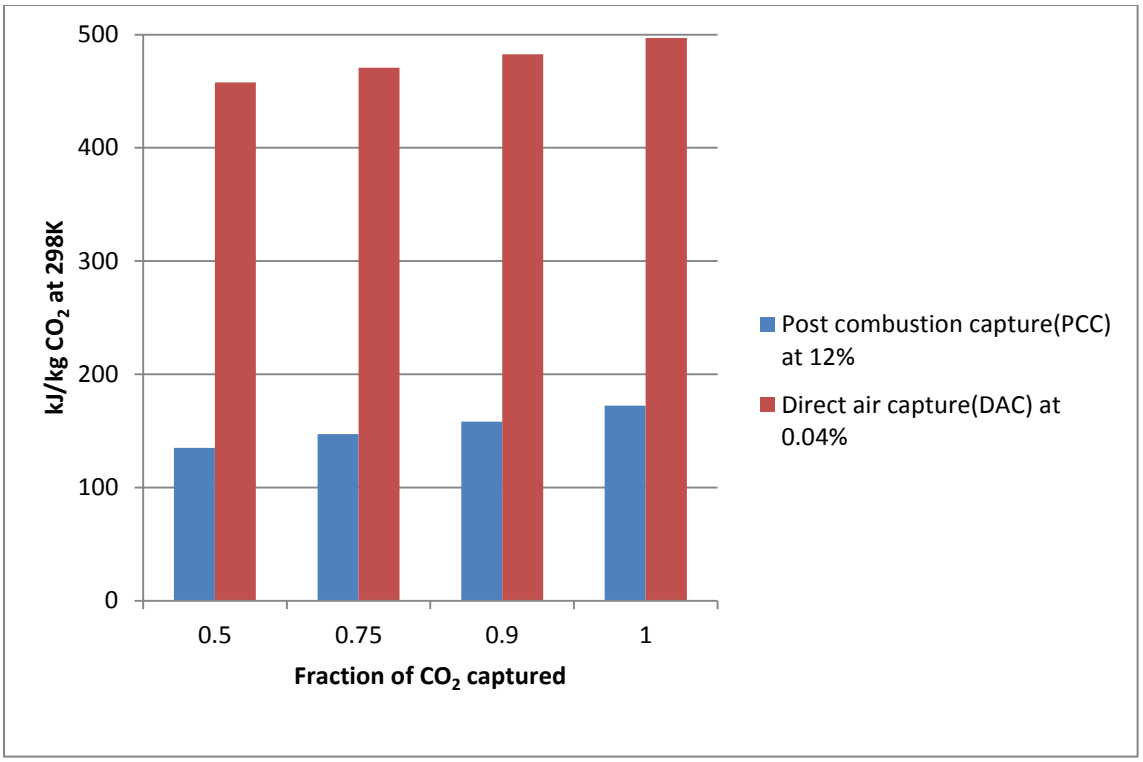

Figure 11. Energy costs needed for separation of flue gases (mainly CO_2) from industries or direct air, based upon entropy of the gases [39]

The other commercial method of recovery of CO_2 from flue gases are absorption based and most common used absorbent is sodium hydroxide (NaOH). Due to the high electro negativity the strong bonding is related with NaOH reacting with potential loadings of CO_2. That high energy creates problems when CO_2 is being removed back during the regeration process. This regeneration of sodium carbonate is a challenging task; along with restoring of sodium hydroxide solution. If one is using thermal decomposition for sodium carbonate, the evaporation of water is simply not attracted economically and makes process impractical. Step 3 which is shown below; is most energy-intensive step because of high energy requirement to break calcium carbonate into CO_2, around 900ºC temperature is needed for breakage. This thermal heat of 900ºC is provided by say natural gas which is burned in oxygen or air. This burning turns out to in producing CO_2 again or need separation unit, hence it becomes illogical.

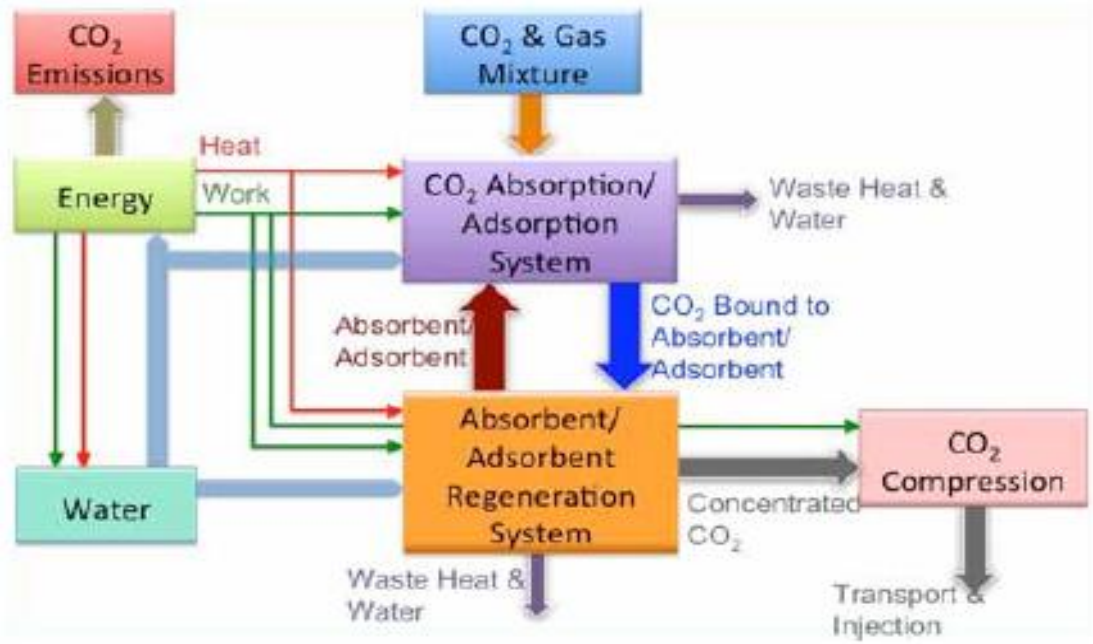

Figure 12 CO_2 capturing process based upon absorption/adsorption process[39]

The capture of CO_2 using sodium hydroxide is illustrated into four steps:

- **Step1** : Formation of Na_2CO_3 (ΔH= -105 kJ/mole).
    - 2 NaOH (solution) + $CO_2 \longrightarrow Na_2CO_3$ (solution) + H_2O
- **Step2**: Formation of $CaCO_3$ and regeration of NaOH (ΔH= -8 kJ/mole).
    - Na_2CO_3 (solution) + $Ca(OH)_2$ (slurry) $\longrightarrow CaCO_3$ (wet solid) + 2 NaOH (solution)
- **Step3**: Release of CO_2 & CaO from $CaCO_3$ (ΔH= 179 kJ/mole).
    - $CaCO_3$ (solid) $\longrightarrow$ CaO (solid) + CO_2 (gas)
- **Step4**: Formation of $Ca(OH)_2$ (ΔH= -65 kJ/mole).
    - CaO (solid) + $H_2O \longrightarrow Ca(OH)_2$ (slurry)

The other type of absorbent consists of amine group for instance MEA monoethanolamine (MEA), diethanolamine (DEA), methyldiethanolamine (MDEA),

diisopropanolamine (DIPA), triethanolamine TEA and other amine groups. The most practical used amine group is MEA. MEA is commercially used for recovery of CO_2 from flue gases at various concentrations, however main problem associates with MEA is corrosion problem. Normally hydrogen sulfide is present in the feed to decrease carbonic acid corrosion; in case of flue gas the hydrogen sulfide is absent. MEA is sensitive to oxygen and SOx that could degrade the activity of these solvent. Flue gas contains approximately 1.5 vol% of oxygen concentration, carbon steel based material is used for manufacturing of any unit, however these carbon steel corrodes due to the presence of oxygen along with MEA. The substitute of carbon steel with other alloys are not cost effective. The presence of SOx in flue gases which reacts with MEA and produces corrosive salts. Practically it is essential to install SOx scrubber in order to prevent expensive MEA solution losses, therefore desulfurization from flue gas is needed. According to standard methods for desulfurization, almost 97-98% of the SOx are being removed from flue gases, however for MEA the concentration of SOx must not exceed approximately 10 ppm. To achieve such low concentration of SOx in flue gas; secondary absorber is essential. The installation of secondary absorber is not attracted due to capital, energy and maintenance costs.

In case of CO_2 capturing from coal power plant starts with absorption column, which is around 40 meters high and 10 meters in diameter. The entering fluids in MEA absorber are carbon dioxde, nitrogen, oxygen and some water vapors. The operating temperature of absorption is 40 to 60°C. The counter current method is implemented; the solution of amine is introduced from top to bottom and gas flows from bottom to top. The concentration of MEA is 25-30% (mole fraction). The treated flue gas leave the absorber from top and CO_2 rich amine solution is moved to stripper process via heat exchanger. In order to avoid water losses which causes variation in molarity of amine solution, the temperature of solvent inlet entering the absorber is opted. The stripper process is operating at 100 to 140°C, at that temperature amine solution releases CO_2. The lean CO_2 solution of amine is transferred again to the absorption column for reuse by heat exchanger. Practically stripping process does not operate perfectly and losses some amount of MEA, therefore water wash is necessary to recovery that small amount MEA solvent. Furthermore at stripping MEA is thermally degraded and it also oxidizes when

comes in contact with oxygen. Resultly, the concentration of MEA is aqueous solution decreases and almost 0.5 to 3.0 kg of MEA needs to be pored for each ton of captured CO_2 [39].

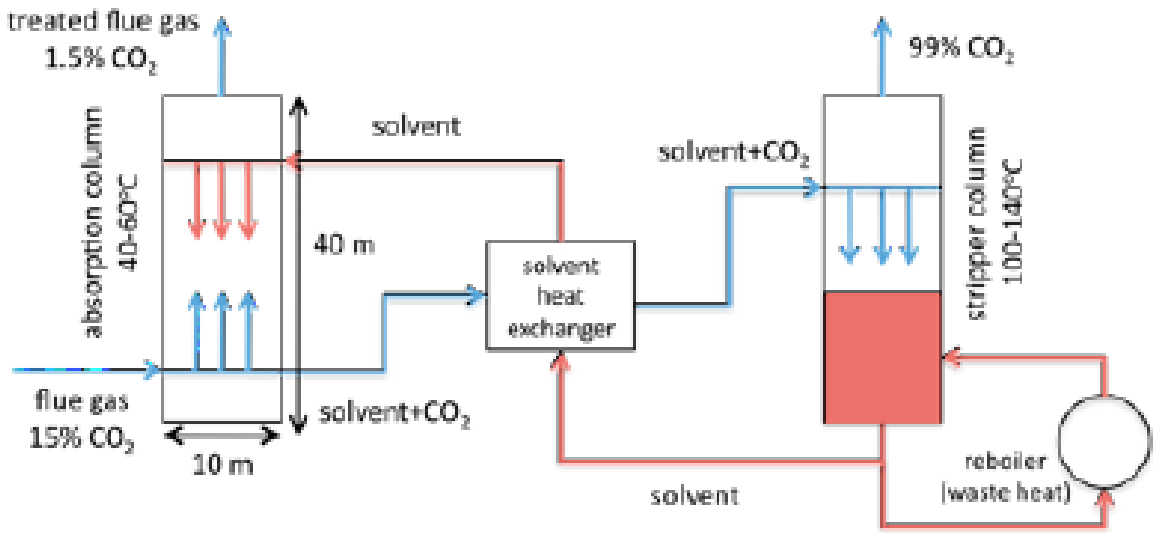

Figure 13 Process flow for MEA based sorption of CO_2 [39]

4.1. Membrane Technologies

Most of the membrane mechanisms are based upon physical or chemical adsorption for instance porosity and affinity. Membranes contains micro-nanoscopic sieves. Under the influence of certain pressure, molecules of different molecular weight passes that sieve and remaining molecules are stopped. Every type of membrane needs driving forces, which could be done by pressure difference, concentration gradient or by electric charges. In case of gas separation most practically used driving force is pressure and concentration gradient. In general, there are two basic types of membrane technologies for CO_2 recovery from flue gases; separation membrane and absorption membrane [40].

4.1.1. Gas Separation Membrane

The working mechanism of gas separation membranes is based on pressure gradient and permeability of various gases that tends to separate these gases. Since this process does not have chemical reactions, the regeneration sorbent is not needed. The membrane separation technology has achieved considerable success to separate CO_2 from low molecules hydrocarbon in natural gas process, petroleum and chemical industries, however separation of CO_2 from flue is under development stage. CO_2 separation from flues gases using separation membrane needs high volume of air to pass through membrane because of low concentration of CO_2 3 to 15%. This leeds to high energy cost of compressor. If two stage membrane are used for better separation, the cost would be double compared to conventional separation process of amine. The transport flux via membrane is given as:

$$J = \frac{P^*}{\delta}\left(xP_f - yP_p\right) \tag{59}$$

Here P^* the permeability of gas, δ the thickness of membrane, P_f and P_p are feed and permeate side pressures. The cross flow scheme of membrane is showed below [41]:

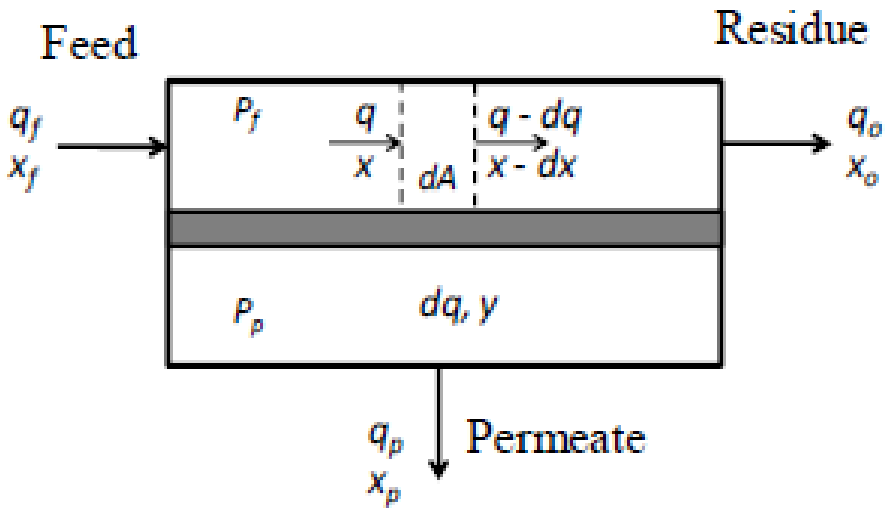

Figure 14 Membrane based CO_2 separation technique [41]

The permeability rate of gases is given as:

$$-ydq = J_{co2}dA = \frac{P^*_{CO2}}{\delta}[xP_f - yP_p]\text{dA} \tag{60}$$

$$-(1-y)dq = J_{N2}dA = \frac{P^*_{N2}}{\delta}[(1-x)P_f - (1-y)P_p]\text{dA} \tag{61}$$

Dividing these equations yields:

$$\frac{y}{(1-y)} = \frac{\alpha(\frac{1-y}{\phi})}{(1-x)-(1-y)\frac{1}{\phi}} \tag{62}$$

Here A is the area of membrane, q the flow rate of gas, α the membrane selectivity P_{CO2}/P_{N2} and ϕ the pressure ratio of feed and permeate. According to Weller and Steiner, the final equation could also be written as:

$$\frac{(1-\theta^*)(1-x)}{1-xf} = \left(\frac{uf-E/D}{u-E/D}\right)^R\left(\frac{uf-\alpha+F}{u-\alpha+F}\right)^S\left(\frac{uf-f}{u-f}\right)^T \tag{63}$$

Furthermore, membrane area is given by Geankoplis:

$$Am = \frac{tqf}{P_f P_{N2}^*} \int_{i0}^{if} \frac{(1-\theta^*)(1-x)}{(f_i - i)\left[\frac{1}{1+i} - \frac{1}{\phi}\left(\frac{1}{1+f_i}\right)\right]} di \quad (64)$$

4.1.2. Absorption Membrane

The absorption membrane uses a liquid sorbent which transports away the CO_2 molecules, diffuses through membranes and hence does not need high pressure compared to gas separation membrane. The prime responsibility of membrane is to act as an interface between the feed gas (flue gas) and liquid sorbent. The configuration of membranes could be parallel hollow fibers, whereas feed gas and sorbent are on the other sides of hollow fibers. This arrangement increases considerably gas-liquid contact area compared to packed absorbers. In addition, the size of the absorber reduces and hence plays integral role in cutting the cost of manufacturing and maintenance cost. Furthermore, it is possible to control fluid flow independently, which reduces operational issues like fouling, foaming and channel formation. The following section discusses about porous and non-porous membrane separately. In porous membrane, gaseous fluid diffuses into pores and then is absorbed by liquid fluid. Therefore, pore size is selected carefully for each species. However, non-porous gaseous fluid dissolves in membrane and then diffuses through membrane; the surface area between both fluids are controlled by flow rates as mentioned above. The selectivity the characterization of solvent must be known and the absorption could be done via physical phenomena or chemical reactions [40, 42].

The selection of adequate solvent and membrane determine operating parameters. The mass transfer of fluid via membrane is avoided at pressure difference of roughly 50 to 100kPa. The rest of process setup is similar to conventional absorption process. The pore characterization and hydrophobicity of membrane are recommended to be gas filled even at elevated temperature say 100 kPa on liquid side. The most commonly available porous membrane are polyolefin based. These types of membranes are inadequate for aqueous absorption solution. For example alkanolamines have lower surface tension for organic fluid. The better hydrophobicity could be achieved by polytetrafluoroethylene (PTFE).

The other way is to use liquid sorption similar to surface tension of water, like CORAL a mixture of amine and salts [43].

Some research work is done related with facilitated transport membrane. The facilitated transport membrane depends upon establishment of complicated or reversible chemical reactions of flue gas species along with species present in membrane. In facilitated transport membrane, the diffusibility and selectivity do play their role. The additional element is specific species interaction with membrane, which is called carriers work as driving force. The driving forces rely on partial pressure difference of species that is to be transferred through membrane. The other important feature of facilitated transport membrane is liquid carrier, which are dissolved in liquid.

The suggested carriers are carbonate, amine and molten salts due to their better affinity and the porous and ion exchange membrane are recommended for support. The supported liquid based membrane are studied in laboratory scale until now [44]. The couple of problems are associated with this type of membrane like stability and volatility of solvent that need to be addressed. Furthermore, as the partial pressure of fed flue gas increases, the selectivity decreases. The behavior happens due to the saturation of carrier also when the pressure increases the permeability of unwanted fluids also increase, hence the wanted species are being bounce back. The selectivity is also affected by thickness of membrane: the lower the thickness the lower will be the selectivity [44].

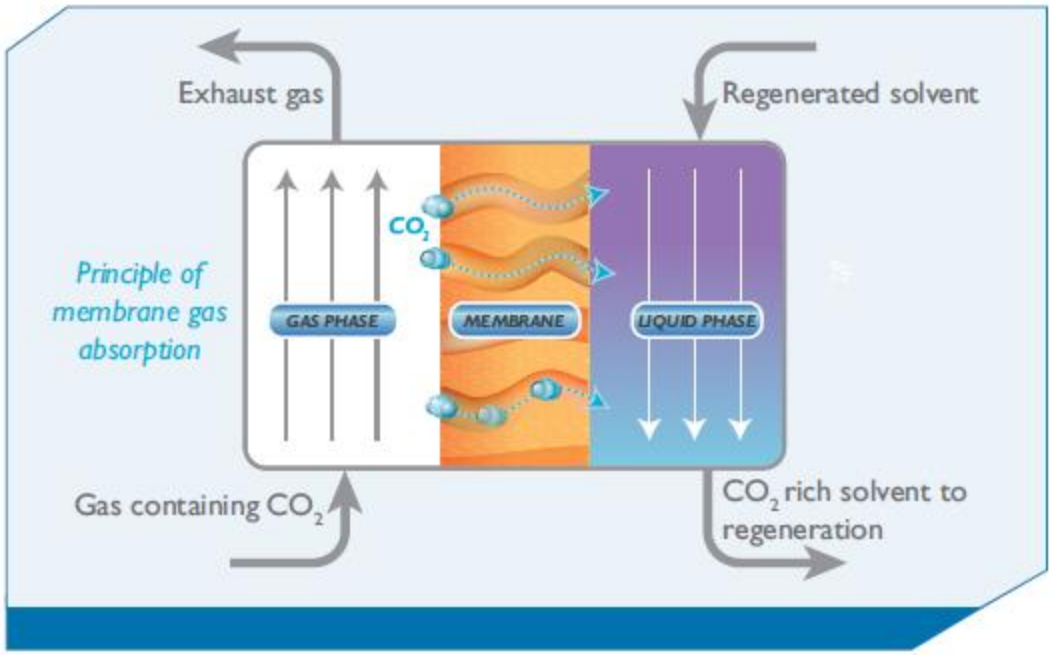

Figure 15 Gas adsorption membrane technique [5].

4.2. Fluidized Bed

Another method of capturing CO_2 from flues gases is using solid sorbents. This sorbent can be used through physical, chemical or with their combination. The properties and thermodynamics of sorbent bed is very important. For CO_2 capturing the most prominent chemicals are amine based and sodium carbonate. These chemicals are placed on to the surface of solid surface where they trap the CO_2 via chemical reactions. If activated carbon or zeolites are used, the physiosorption is achieved. The advantage of using solid sorbent are elucidated below:

- The handling of material is easy.
- Environment friendly.
- Moderate/good CO_2 capacity.
- The cost of regeneration is low.
- Tendency to control unwanted pollutant.

The different types of contactors between flue gas and solid sorbent could be used, such as fixed bed, moving bed, bubble column and fluidized bed. Depending upon the activity, selectivity and capacity for CO_2, various solids can be utilized to react with CO_2 which yields desired product from the process. Then the sorbent is being regenerated and CO_2 is recovered. During the adsorption process, the CO_2 is adsorbed by zeolites or activated carbon and in regeneration step; the CO_2 is recovered by either pressure swing or temperature swing. It is observed that temperature swing adsorption has longer regeneration duration as compare to pressure swing adsorption.

The prime focus of adsorption process is high surface area for flue gas contacting with sorbent and selectivity for CO_2. This high surface area in case of chemical reaction is achieved by alumina or silica. The selectivity is accomplished by amine (polyethylene amine) and sodium (sodium carbonate) based reactants. The example of sodium based sorbent is given by basic reaction of sodium carbonate as mentioned below. The regeneration is done by temperature swing and it produces CO_2; which is later cooled and compressed [45].

$$Na_2CO_3 + H_2O + CO_2 \leftrightarrow 2NaHCO_3 \quad (65)$$

The example of amine based sorbent, i.e. polyethylene amine (PEI) with nonporous support of polymer, which is also known as molecules basket sorbent (MBS). This is a new phenomenon in that PEI is located on the porous material say MCM-41 or SBA-15 for increasing the accessibility towards sites, the other advantage is to increase mass transfer efficiency by increasing interface of flues gas and PEI. The main advantages are listed below:

- Better CO_2 selectivity and capacity.
- Improve sorption and desorption rate (energy cost saving).
- Stable and short regeneration cycle.
- Low corrosion and overall low energy cost.

The fluidized bed technology for capturing of CO_2 from flue gas has numerous possible advantages for instance it offers respectable mixing of gas and solids, which gives better heat transfer due to high surface area between heat exchange tube and bed. We know that the adsorption step of CO_2 is exothermic, whereas the desorption step needed for sorbent regeneration is endothermic. Therefore, it is very important to obtain uniform distribution of temperature and better heat transfer. This uniform distribution of temperature is not possible in case of fixed bed and creates unwanted hot spots.

The sorbent may consist of different chemicals for instance potassium, sodium and calcium based. In case of sodium or potassium, the reactions of adsorption and regeneration are mentioned below:

$$M_2CO_3 + CO_2 + H_2O \rightarrow 2MHCO_3 + Heat \tag{66}$$

$$2MHCO_3 \rightarrow M_2CO_3 + CO_2 + H_2O \tag{67}$$

Here M is representing Na and K. Let us discuss the mathematical model for potassium based sorbent using bubble fluidized bed. The CO_2 present in flue gas enters to the adsorber and creates turbulence in fluidized sorbent bed. After the chemical reaction of potassium and CO_2, the product of adsorbed is transferred to regeneration step. In regeneration the inert gas, steam or other type of gases enters the system and fluidizes the

CO_2 rich sorbent bed. Due to the reverse reaction, CO_2 is being separated and regenerated bed is sent back to adsorption process. The equation for adsorber and regenerator is [46]:

$$\frac{dp_{bi}(x)}{dx} + \sum_{k=1}^{2} \alpha_{ik}(x) P_{bk}(x) - \alpha_{i3}(x) = 0 \ (i = 1,2) \tag{68}$$

$$\alpha_{i1}(x) = \delta_{1i}\left[\frac{F_1 + K_1^*\left(1-\psi_1(x)R_{f12}\right)}{W_1 R_1(x)} + \frac{dR_1(x)}{R_1(x)dx} - \frac{3}{x}\right] - \alpha_{2i}\frac{F_1}{W_2 R_2(x)} \tag{69}$$

$$\alpha_{i2}(x) = -\delta_{1i}\frac{F_{f10}}{W_1 R_1(x)} + \delta_{2i}\left[\frac{F_{f10} + K_2^*(x)\left(1-\psi_2(x)R_{f2}\right)}{W_2 R_2(x)} + \frac{dR_2(x)}{R_2(x)dx} - \frac{3}{x}\right] \tag{70}$$

$$-\alpha_{i3}(x) = \frac{\delta_{1i}F_0 p_0(x) + R_{a1}p_{ai}(x)}{W_i R_i(x)} \tag{71}$$

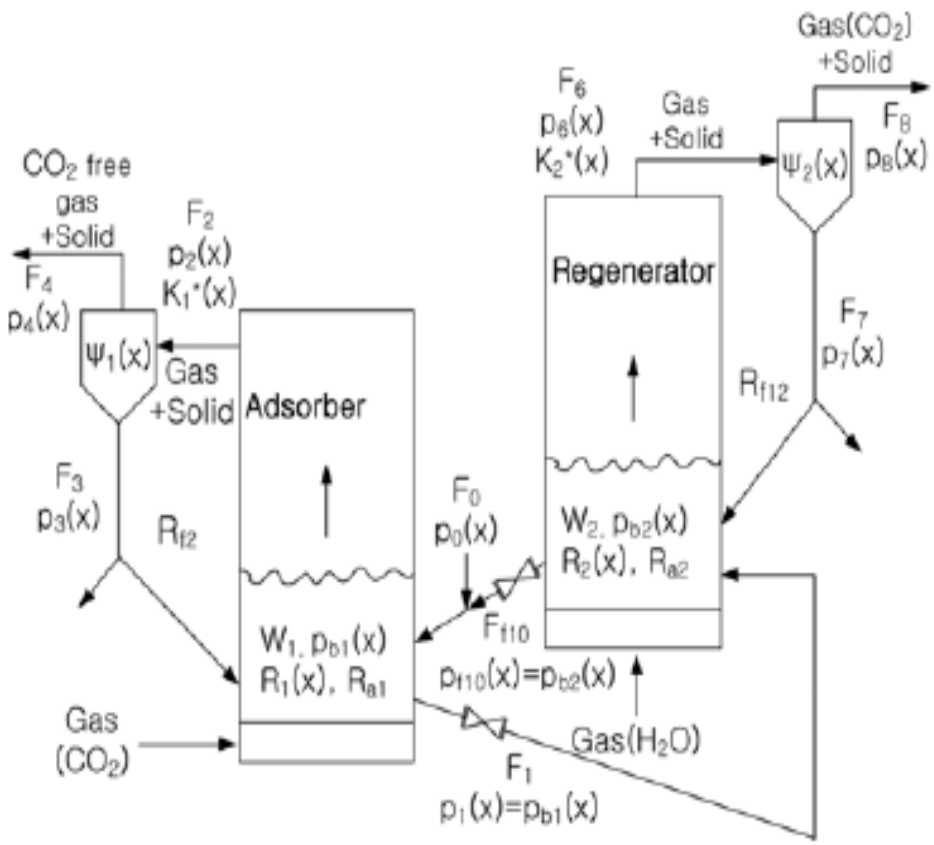

Figure 16 Fluidized adsorption of CO_2 and desorption in regeneration reactor [45]

One of the promising methods of recovering CO_2 from flues gas is by fluidized bed using lime carbonation-calcination cycle, also known as calcium looping. The vital importance

of calcium looping method for post combustion is capturing of CO_2 at elevated temperatures, which is around 873 to 973K. This high temperature facilitates calcite calcium carbonate during regeneration process by recovering energy from exothermic carbonator.

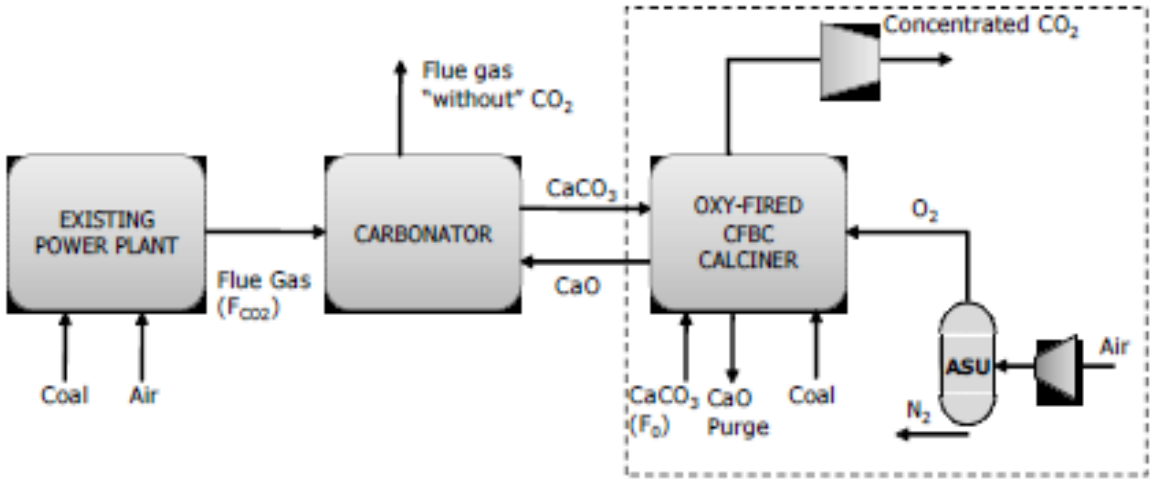

Figure 17 Calcium looping process for CO_2 capturing and desorption [47]

In carbonator CaO reacts with CO_2 and converts into $CaCO_3$ partially, the product of carbonator is headed towards second fluidized bed; where regeneration process happens. During the calciner process, the coal is burned along with O_2 and CO_2 around 1173.3 temperatures. This step produces sufficiently heat needed to break $CaCO_3$ into CO_2 and CaO. Oxygen for calciner is mainly provided by air separator. The CO_2 captured from flue gases is sent to compressor, where it is compressed and purified (if needed) and later it is being stored. Calciner consumes approximately 35 to 55% of total energy of the plant because the reaction of $CaCO_3$ is endothermic, and therefore, it is also necessary to heat the flues gases. The heat losses is recovered at carbonator as carbonation heat, the calciner and carbonator recycle the heat losses and works efficiently hence key unit here is calciner.

There are some advantages of using fluidized bed technology for carbonator. They are similar to fluidized bed combustors. Therefore, mechanical cost might be minimized for looping technology (carbonation-calcination loop). Furthermore, fluidized bed are also

available in supercritical power plants, making Ca looping possible. There is lack of publications on Ca looping. Therefore, the performance of sorbent, the selectivity and regeneration stability need to be studied further both experimentally and by simulation [47].

The main concerns with fluidized bed process are elevated capacity, attrition resistance, stability, cost and regenerability. The stability of sorbent structure and functionality must be maintained during repeated regeneration steps, because sorbent may get erosion/degradation due to physical abrasion and chemical reactions. Therefore, sorbent must have high resistance to thermal and mechanical resistance along with good capacity at adequate time frame of about 2 to 8 seconds. All these features of sorbent are needed to be answered in near future at acceptable cost [48].

5. Research Methodology

The experimental setup is divided into two parts: absorption experiments and precipitation experiments.

5.1. Absorption Setup

For absorption batch experiments in open vessel stirred tank with a 86-liter volume was used. The vessel was placed on vertically movable stand, whose position was adjusted electrically. The impeller was positioned inside the vessel in such a way that it should not touch the sparger at the bottom of vessel. The feed of calcium carbonate suspension was poured from the top. Then, the feed of oxygen and nitrogen was introduced through the bottom of vessel with the aid of the sparger. The nitrogen was used to make the solution unsaturated with respect to oxygen and other gases. The temperature of the vessel was controlled at 10ºC by a heat exchanger coil connected to a temperature controller. The gas flow rate of oxygen/nitrogen was adjusted by a flow rate meter. Rotation speed of the impeller were varied in the experiments.

Figure 18 Experimental setup for absorption process.

5.2. Precipitation Setup

The precipitation experiments are done in closed environment. The open vessel of 4 liters was used. Initial solution contains magnesium hydroxide suspension. The impeller was placed near to the bottom and the temperature was controlled by the jacket of the vessel. The feed flow rate of carbon dioxide was controlled with a gas flow controller. The growth rate and particle size distribution were measured by MTS PSyA 5.23. For ion chromatographic, particle size distribution and total organic carbon analyses, samples from the vessel were taken after certain time intervals with the aid of syringe. Total carbon, TC, was calculated by:

$$TC = TOC + IC = CO_3^{2-} + HCO_3^{-} + CO_2(l) \quad (72)$$

The calculation of other species concentrations like HCO^{-}, CO_3^{-2} and OH^{-} is based on following equations. Here Methyl Orange and Phenolphthalein are denoted by MO and FF, the intial volume is V_1 and V_2 for each indicator and V_3 is total volume.

$$\boldsymbol{FF}=V_1*n*1000/V_3 \tag{73}$$

$$\boldsymbol{MO}=V_2*n*1000/V_3 \tag{74}$$

Table 1 The calculation method to figure out concentration of HCO^{-}, CO_3^{-2} and OH^{-} . Here Methyl orange and phenolphthalein are indicators.

MO/FF	HCO_3^-	CO_3^{2-}	OH^-
FF=0	MO	0	0
2FF<MO	MO-2FF	FF	0
2FF=MO	0	FF	0
2FF>MO	0	(MO-FF)	2FF-MO
FF=MO	0	0	MO

Figure 19. Experimental setup for precipitation process.

6. Results and Discussions

6.1. Absorption

6.1.1. Absorption of Oxygen in Water

Initially the absorption experiments were performed with simple oxygen and water. The flow rate of the gas feed was kept constant as 6 liter/min. The temperature of the system was 10ºC. t_0 is the initial time of starting of experiments and the C_0 is the initial concentration of oxygen at time t_0. The initial saturation level denoted by S_0 is shown in Table 1. The effect of rotation speed of the mixer are observed on absoption of oxygen into water, the rotation speeds were varied from 237, 365 and 465 rpm randomly to introduce turbulence. At low rotation speed of 237 rpm, the achieved final saturation level was 95.3 % from 5.1%, and final concentration of feed is 10.9 mg/l from initial solid concentration of 0.58 mg/l. As the rotation speed increased say 465 rpm, the optimum saturation is accomplished 95 %. The initial saturation level was high 9.8% due to some experimental error. If the initial saturation was low say 5.1 % then achieved (final) saturation might be higher than 97 %. Table 2 shows the details elucidation of experimental values of oxygen absorption. The oxygen mass transfer coefficient [22] and power input per unit volume of liquid (P/V) calculated values and graphs are presented later.

Table 2. Absorption of oxygen in pure water at 10 ^{0}C with flow rate of 6litres/min.Here N is rotation per minutes(rpm), Q is flow rate in litres/min, T is temperature in Celcius, U is conductivity, t_0 and t_f are initial and final time in minute, C_o andC_f are initial and final concentration is mg/l, S_0 and S_f are initial and final saturation, kLa is oxygen mass transfer coefficient, and P is power in volts

N	Q	T	U	t_0	C_0	S_0	t_f	C_f	S_f	kLa	F_p	P	P/V
237.00	6.00	10.00	1.47	0.63	0.58	5.10	0.64	10.89	95.30	0.005	0.873	21.648	248.831
365.00	6.00	10.00	4.20	0.65	0.63	5.60	0.65	10.93	95.70	0.010	2.490	95.121	1093.350
465.00	6.00	10.00	6.98	0.66	1.11	9.80	0.66	10.86	95.00	0.014	4.137	201.331	2314.154

The response curves of oxygen in water at (a) 237 rpm and k_La value of 0.005131s^{-1} (b) 365 rpm and k_La value of 0.0104 s^{-1} and (c) 465 rpm and k_La value of 0.0145 s^{-1} are shown below:

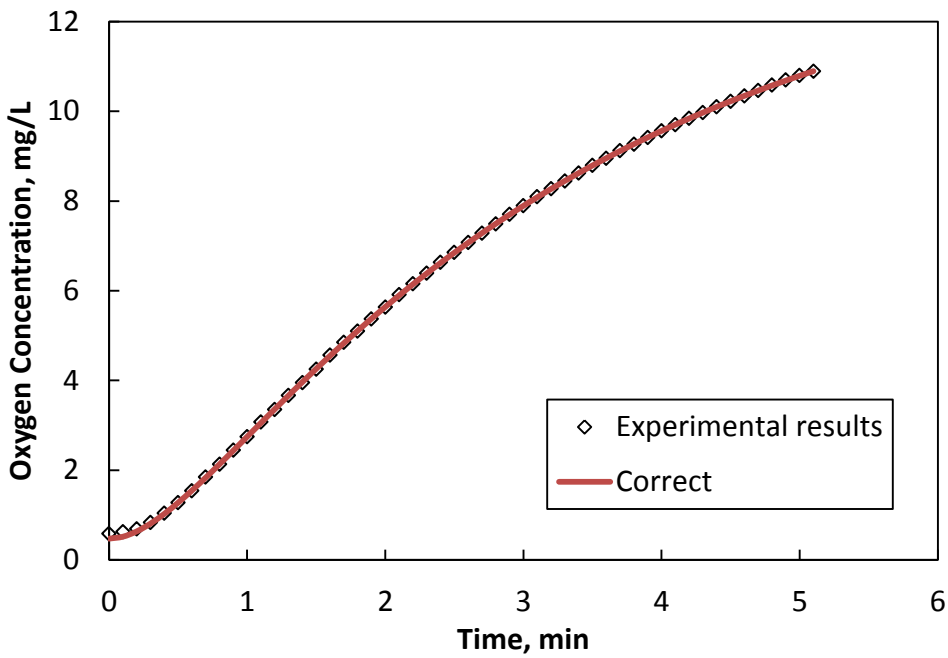

Figure 20 Oxygen concentration in mg/l as a function of time in minutes at 237 rpm. The fitting from response curve resulted in k_La value of 0.005 s^{-1}.

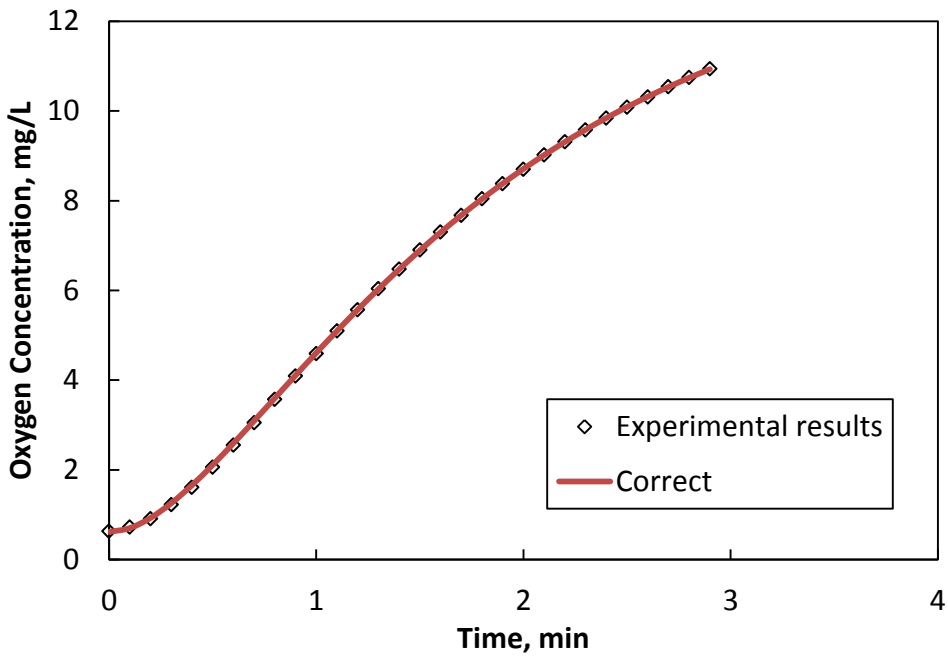

Figure 21. Oxygen concentration in mg/l as a function of time at 465 rpm. The fittineg from the response curve resulted in k_La value of 0.01 s^{-1}.

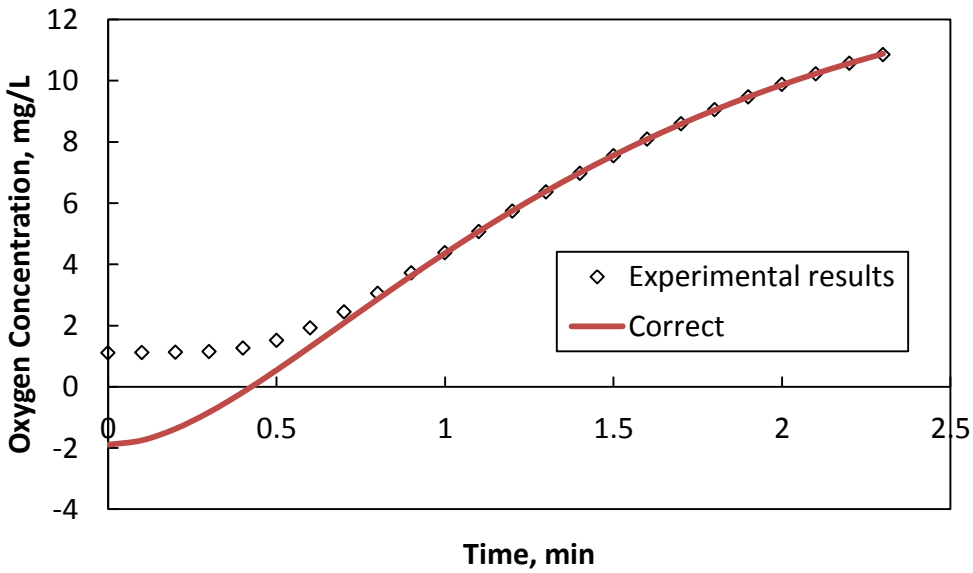

Figure 22. Oxygen concentration in mg/l as a function of time with rotation speed of 365 rpm. The fitting from the response curve data resulted in k_La value of 0.01 s^{-1}.

The calculated k_La and P/V values for oxygen absorption into water are presented in Appendix. The graph of k_La and P/V is:

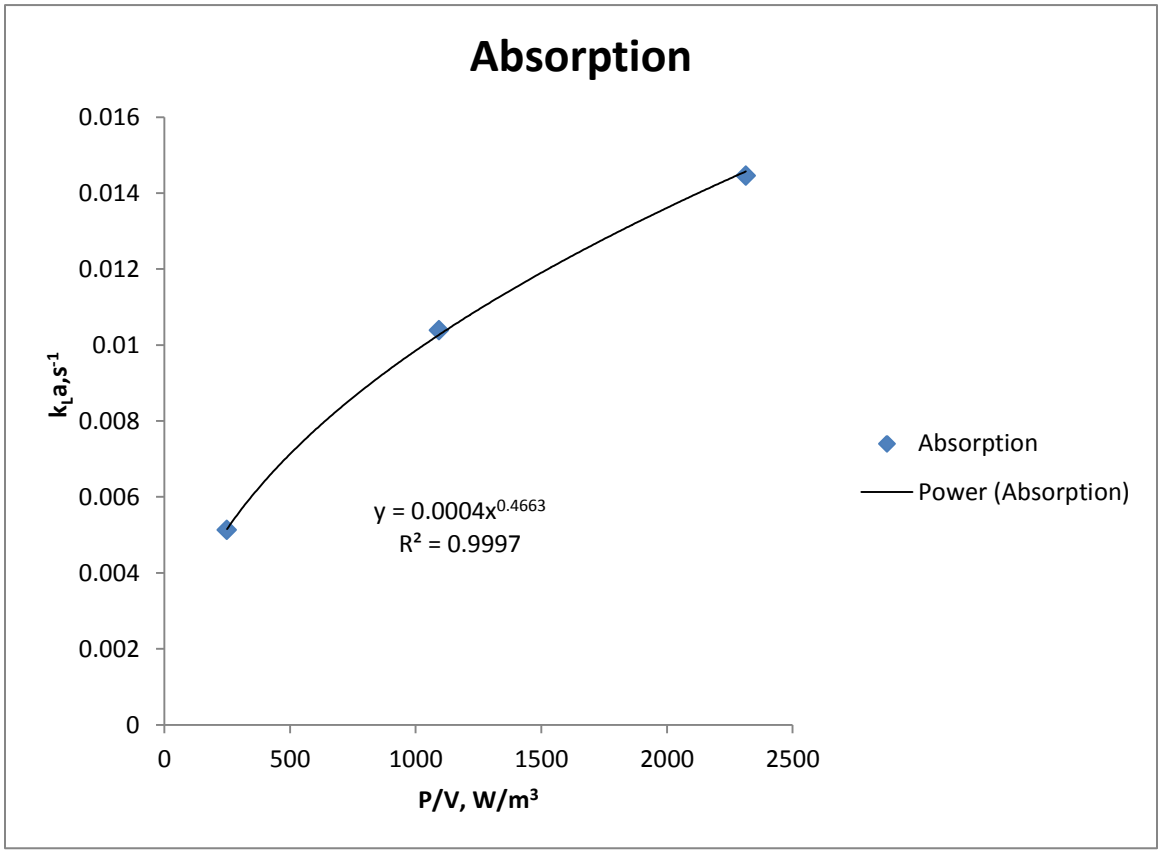

Figure 23 Absorption of oxygen in pure water, the value of k_La is $0.014s^1$ at 2500 W/m^3 .

6.1.2. Absorption of Oxygen in Quartz Suspension

The concentration of quartz used for absorption experiments was 174 g in 87 litre and temperature was the same as in previous experiments, i.e. 10ºC. The flow rate was again kept contant at 6 litre/min, the used rotations speeds were 365, 418 and 464 rpm respectively. Each experiment was performed twice to verify the reproducibility of the experiments. The obtained results are showed in table 3 below:

Table 3. Absorption of oxygen in quartz suspension. Here N is rotation per minutes(rpm), Q is flow rate in litres/min, T is temperature in Celcius, U is conductivity, t_0 and t_f are initial and final time in minute, C_o andC_f are initial and final concentration is mg/l, S_0 and S_f are initial and final saturation, kLa is oxygen mass transfer coefficient, and P is power in volts.

N	Q	T	U	t_0	C_0	S_0	t_f	C_f	S_f	kLa	F_p	P	P/V
365	6	10	4.00	16:02	0.63	5.5	16:05	11.03	96.5	0.010	2.371	90.595	1041.326
365	6	10	4.00	16:18	0.63	5.6	16:21	10.96	95.8	0.009	2.371	90.595	1041.326
418	6	10	5.35	16:35	0.70	6.2	16:37	10.95	95.9	0.013	3.171	138.738	1594.686
418	6	10	5.35	16:48	0.70	6.2	16:51	11.08	96.8	0.012	3.171	138.738	1594.686
464	6	10	6.70	17:02	1.00	17.04	17:04	10.90	95.4	0.015	3.971	192.843	2216.588
464	6	10	6.70	17:13	1.00	17.15	17:15	10.99	96.1	0.014	3.971	192.843	2216.588

The response curves of measured oxygen concentration at each rotation speed of mixer are shown in the following section.

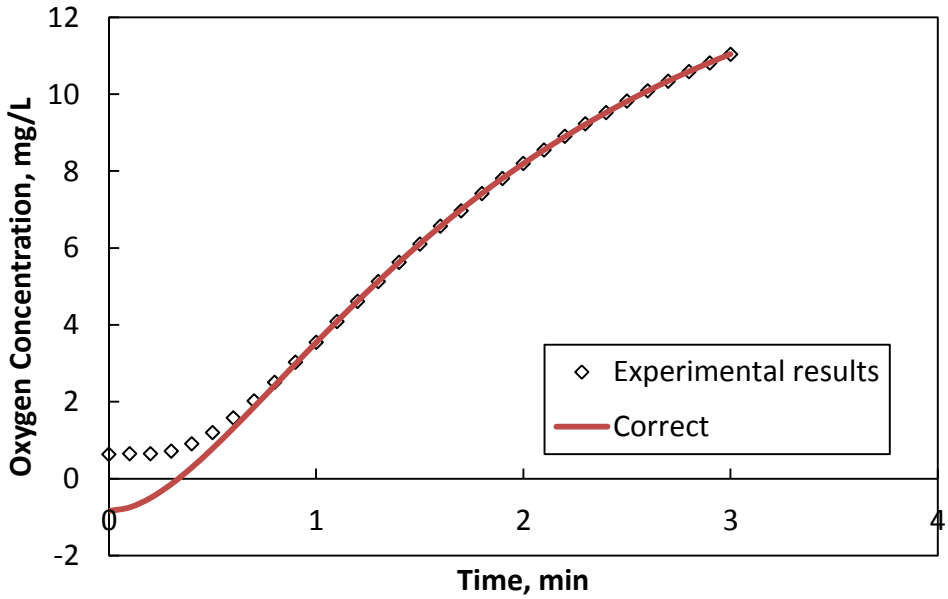

Figure 24 Absorption of oxygen in 174 g of Quartz in 86 L suspension at 365 rpm. The fitting from the response curve resulted in k_La value of $1E^{-4}$ s^{-1}.

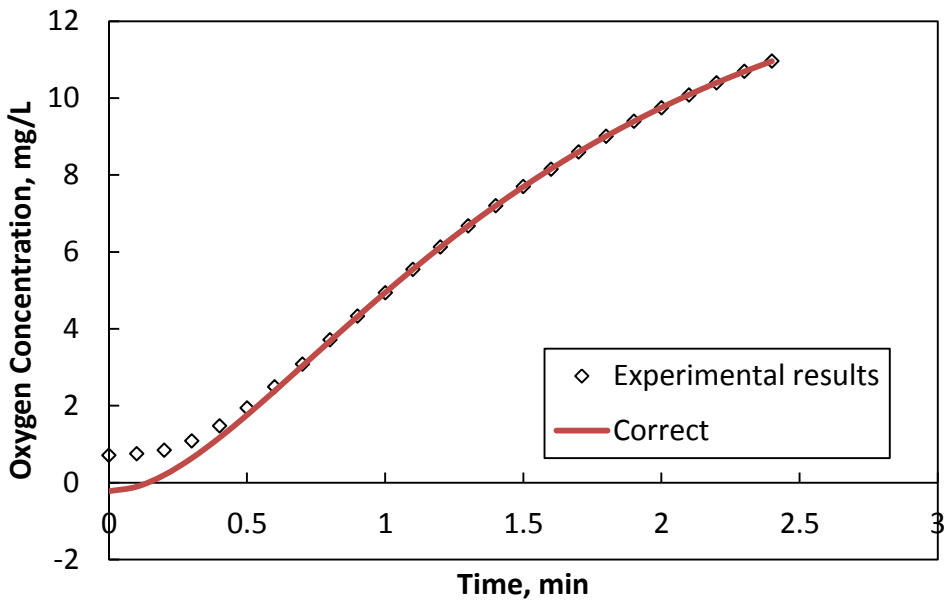

Figure 25 Absorption of oxygen in 174g of Quartz suspension at 418 rpm. The fitting from the response curve resulted in k_La value of $2E^{-6}$ s^{-1}.

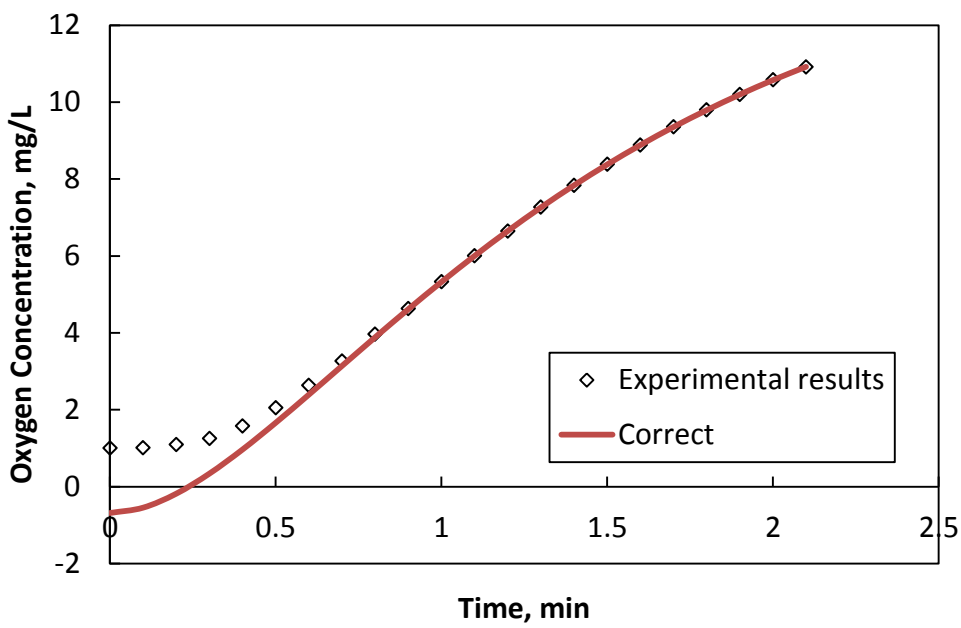

Figure 26 Absorption of oxygen in 174 g of Quartz suspension at 464 rpm. The fitting from the response curve resulted in k_La value of $1E^{-4}$ s^{-1}.

The calculated k_La and P/V values for oxygen absorption into quartz suspension is shown in Appendix A. The graph of k_La as a function of P/V is depicted in the following figure.

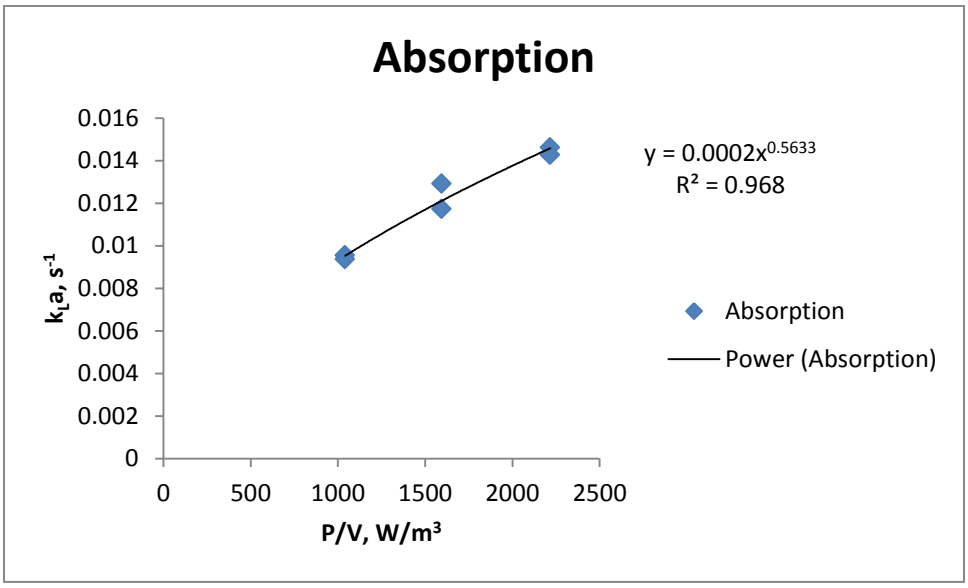

Figure 27 Absorption of oxygen in 174g of Quartz suspension. The value of k_La is 0.013 s^1 at 2400 W/m^3.

6.1.3. Absorption of Oxygen in $CaCO_3$

After oxygen absorption experiments, we introduced calcium carbonate solid particles. For $CaCO_3$ particles, the rotation speed ranges varied from 236 to 466 rpm, the gas volume flow rate was kept constant at 6 litre/min, and the initial saturation varied between 6 % and 9.3 %. Therefore, ogygen concentration varied approximately 95% of the maximum theoretical oxygen concentration variation with initial 0% oxygen concentration. The concentration of calcium carbonate varied from 17.4 to 2382 g and two size fractions were used: size fraction with average size of 5 µm and more coarse size fraction classified with 45 and 63 µm sieves. The detail descriptions of used solid concentrations and particle size fractions of figure 28 to 33 are presented in Appendix A. The graph of k_La as a function of P/V for oxygen absorption into $CaCO_3$ suspension and various concentration and particle size are:

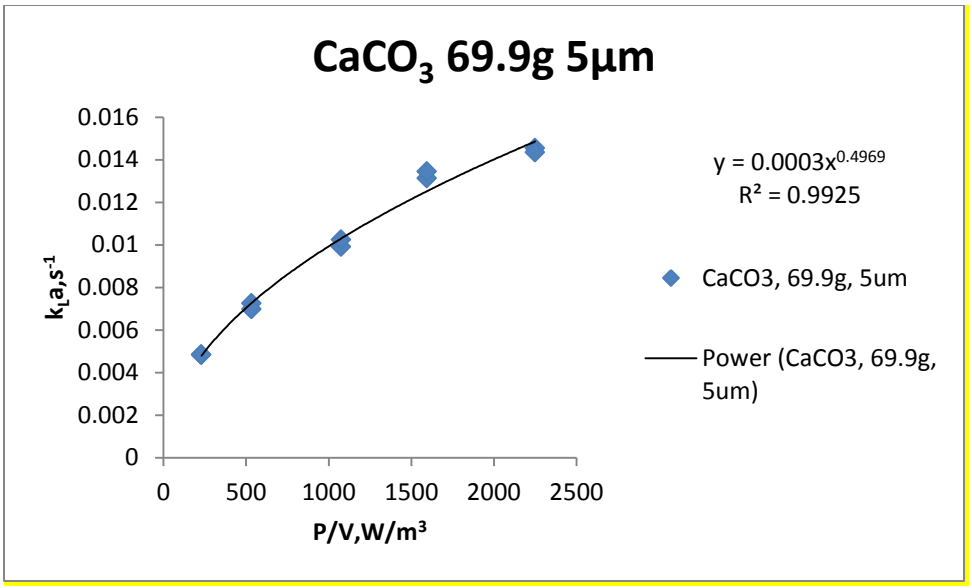

Figure 28 k_La value is $0.014s^{-1}$ at $2250W/m^3$

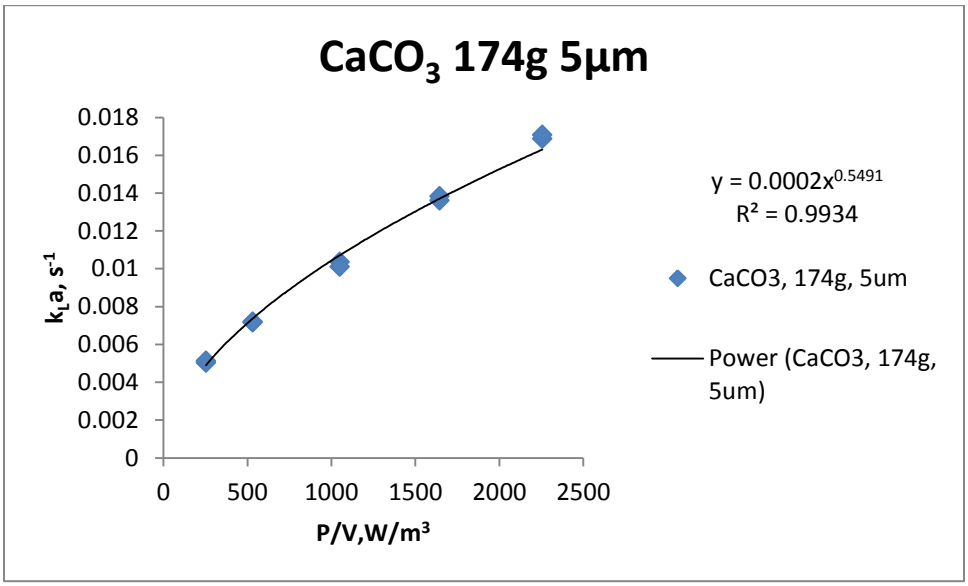

Figure 29 k_La value is $0.016s^{-1}$ at $2256W/m^3$

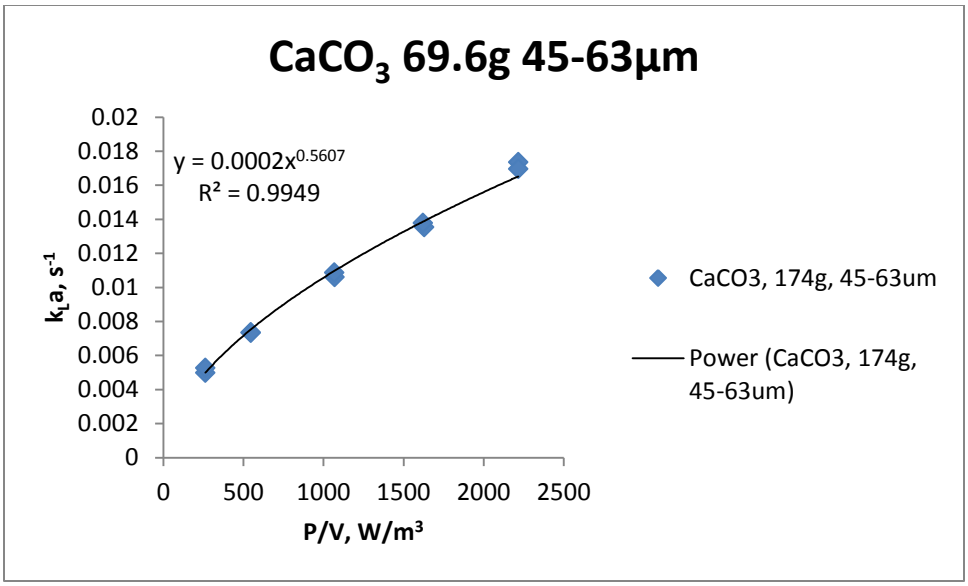

Figure 30 k_La value is 0.017s^{-1} at 2216W/m^3

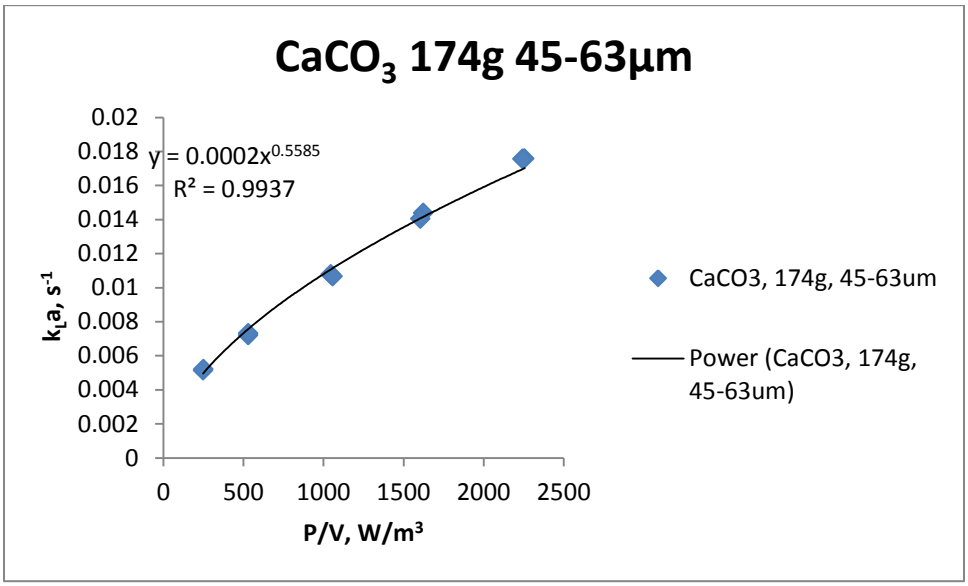

Figure 31 k_La value is 0.018s^{-1} at 2242 W/m^3

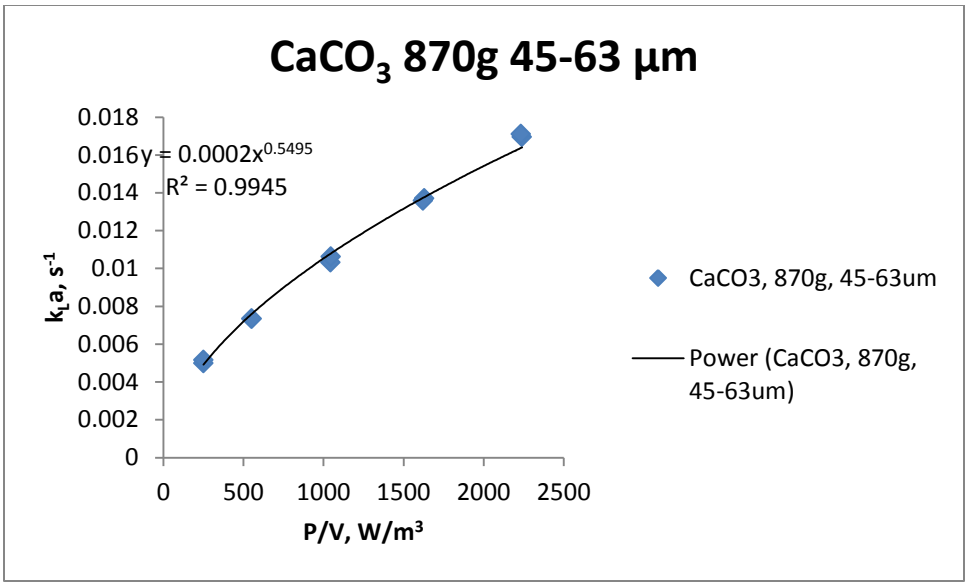

Figure 32 $k_L a$ value is 0.017s^{-1} at 2240W/m^3

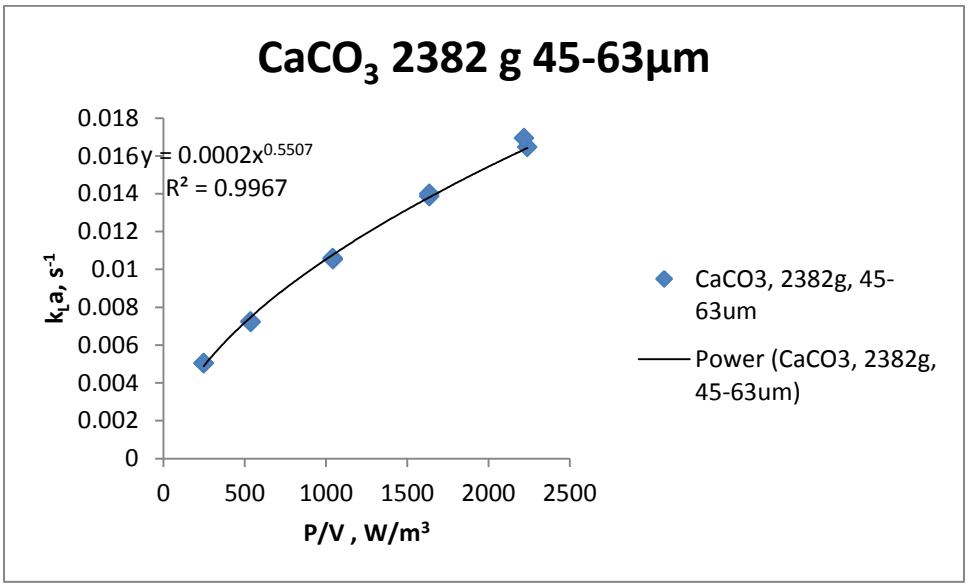

Figure 33 kLa value is 0.017s^{-1} at 2220W/m^3

The absoption results of $CaCO_3$ are plotted in above figures from 28 to 33. As the concentration of calcium carbonate particles increases, higher rotation speeds are required in order to provide more uniform suspension in the open vessel. In Figure 28 and 29, the volumetric mass transfer coefficient value is slightly higher at low concentration

of calcium carbonate. This means that oxygen absorbs faster into the suspensions containing less particles. However, this difference is not significantly great: at 69.6 g concentration of $CaCO_3$ the obtained k_La was 0.014 s^{-1}, whereas at 174 g of $CaCO_3$ k_La is 0.0165s^{-1} approximately.

In figures 30 to 33, the concentration of calcium carbonate has increased from 17.4 g to 2382 g along with larger size fraction between 45 and 63 μm. The results show that with an increase in the concentration together with an increase in rotation speed the achieved k_La values are same. The oxygen is dissolved into the liquid almost at the same rate with low or high concentrations of calcium carbonate.

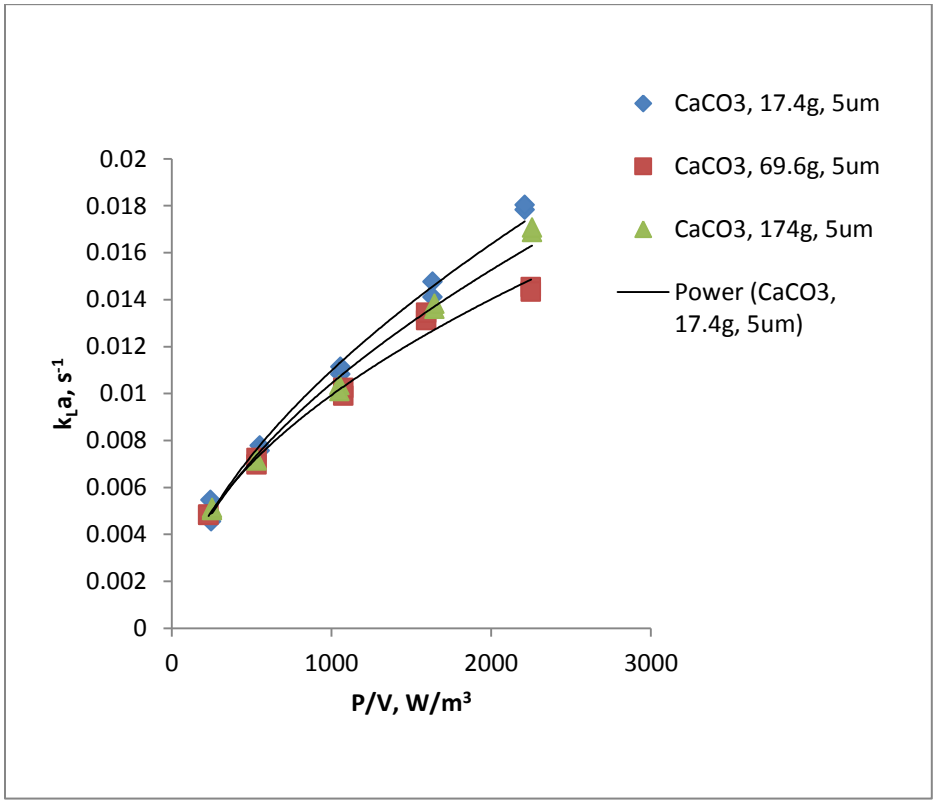

Figure 34 Volumetric flow rates of 17.4g,69.9g and 174g of $CaCO_3$ at particle size of 5 μm. The minimum and maximum values of k_La are 0.014s^{-1} and 0.018s^{-1} at approximately 2250W/m^3.

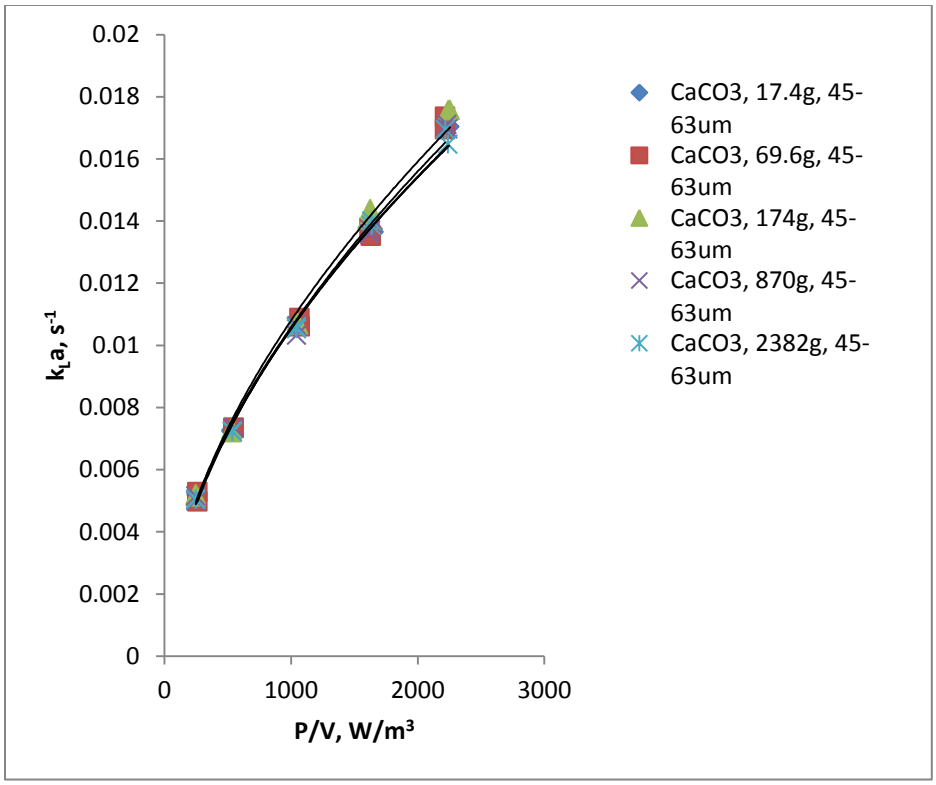

Figure 35 Volumetric flow rates of 17.4g,69.9g, 174g,870g and 2382g of $CaCO_3$ at particle size of 45-63 μm. The minimum and maximum values of k_La are 0.016s^{-1} and 0.0182s^{-1} at approximately 2230W/m^3.

6.2. Precipitation

6.2.1. Ionic chromatography, Titration and TC Analyser

The result of magnesium concentration in part per million (ppm) were analyzed with ionic chromatography. The standard solution of 10, 30, 50, 70 and 100 ppm of magnesium is used for calibration and validation of device. The summary of these results are shown in Appendix B. The graphical representation of magnesium at various concentration and used rotation speeds will be shown later. The titration by 0.2 N solution of HCl is used for analyses of OH^-, HCO_3^- and CO_3^{-2} ions. The used indicators were phenolphthalein, bromocresol green and methyl red.

The TOC (total organic carbon) analyser was used to measure the dissolved total carbon concentration in the solution. The average value of mean concentration was used, in order to be sure about results. The detailed results of TC Analyser is also listed in Appendix B.

6.2.2. Reaction Kinetics of Magnesium Hydroxide

The reaction kinetics of magnesium hydroxide under the influence of CO_2 was studied. The concentration of magnesium hydroxide was kept constant as 100 g, whereas the used rotation speeds were 560, 650 and 750 rpm and gas flow rate 1 and 9 L/min. The dissolution and dissociation of magnesium hydroxide were observed as a function of flowrate of CO_2 and rotation speed. If the dissociation is high, the reaction rate will be higher with CO_2 and as a result total inorganic carbon concentration will be higher. In figure 36 with rotation speed of 560 rpm and CO_2 flow rate of 1 L/min, the dissolution of magnesium hydroxide could be monitored by measuring magnesium ion concentration. The maximum achieved concentration was 0.25 mol/litre at 40 min, afterwards it decreased. The achieved TC was unstable and maximum concentration at 40 min is 0.12 mol/L. In figure 37, the only flowrate of CO_2 is increased to 9 litre/min and keeping rotation speed constant at 560 rpm. It is observed that dissociation rate of magnesium hydroxide is directly proportional to feed rate of CO_2: the maximum molar concentration of magnesium ion was 0.3 in 30 minutes which is higher than with gas flow rate of 1 L/min of CO_2. The achieved TC is slightly higher and has increased to higher 0.15 molar concentration from the previous 0.12 molarity. As shown in both figures, it is clear that the increase in CO_2 feed will increase TC and Mg concentration.

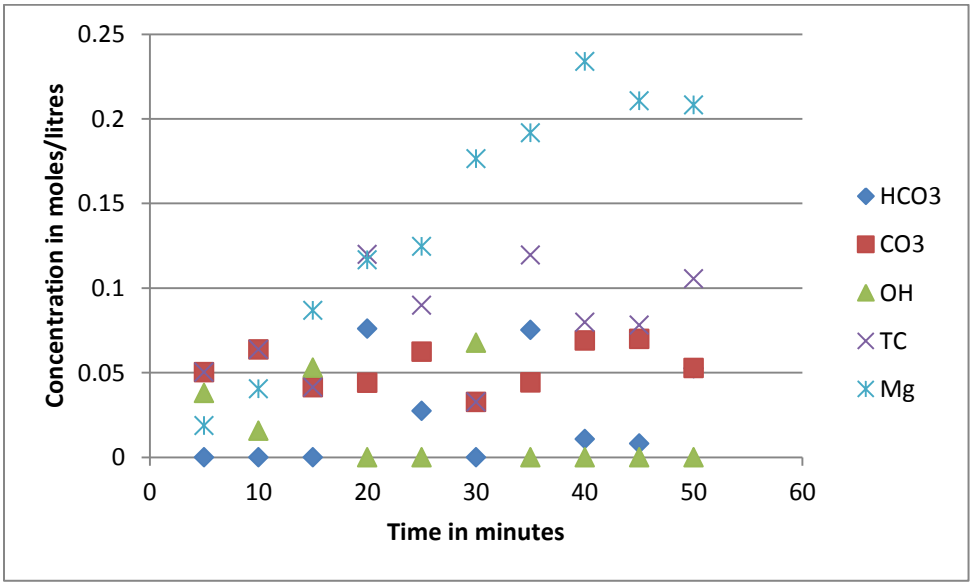

Figure 36 Molar concentration of species over time with rotation speed of 560 rpm and CO_2 feed rate of 1 L/min.

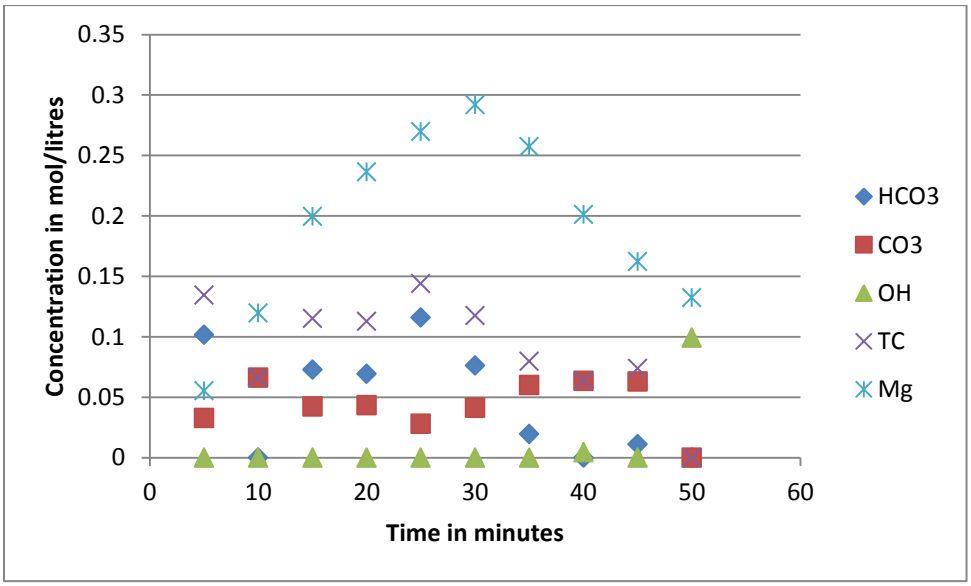

Figure 37. Species concentrations over time with 560 rpm and 9 L/min CO_2 feed rate.

In figure 38, the CO_2 flow rate is kept constant at 1 L/min. When the rotation speed of propeller stirrer was increased to 650 rpm, the maximum molar concentration of TC was 0.09 at 50 min. Unfortunately the Mg data is missing due to experimental error. Therefore, it is hard to say the clear effect of rotation speed on Mg concentration evolution. In figure 39, again the flow rate is kept constant at 1 L/min of CO_2, and used rotation speed is higher, i.e. 750 rpm. The maximum achieved molar concentration of Mg ion and TC were 0.08 and 0.09, respectively. According to the TC analyser the obtained results are almost constant compared to calculated TC and maximum TC value by analyser was 0.06 at 30minutes.

It is also noted that at higher rotation speeds of 650 and 750 rpm with 1 L/min feed of CO_2, the dissociated of magnesium hydroxide is low and the achieved concentration of Mg and TC is less than 0.1 mol/L. With the lowest rotation speed of 560 rpm and 1 L/min feed of CO_2, the maximum value of Mg and TC were 0.25 and 0.12 mol/L. This behavior predicts that as the rotation speed is increased, the CO_2 starts to release from the system and does not have appropriate contact with dissolved magnesium hydroxide. Due to short

residence time magnesium hydroxide dissociation decreases. In order to keep the CO_2 into the system at higher rotation speed, it is favorable to use higher pressure.

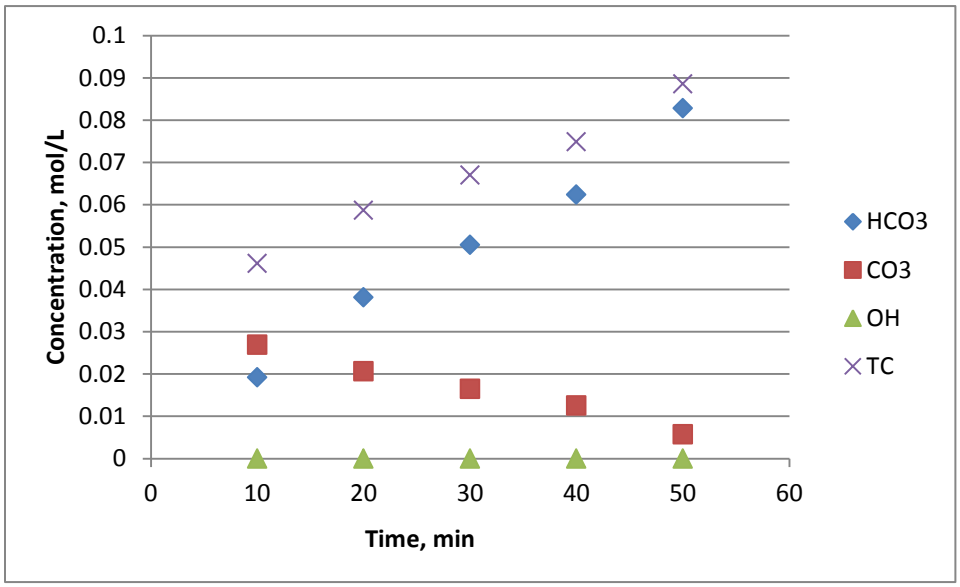

Figure 38. Precipitation with 650 rpm and 1 L/min CO_2 feed rate.

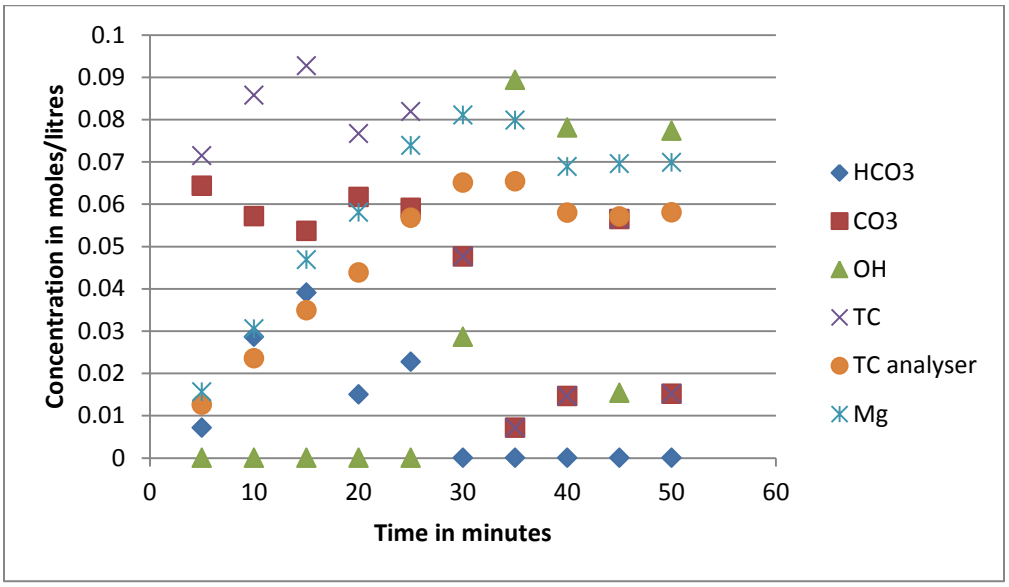

Figure 39. Precipitation with 750 rpm and 1 L/min CO_2 feed rate.

7. Conclusion

The research topic of this work was to investigate mass transfer of oxygen absorption in stirred tank and reaction and precipitation kinetics of magnesium carbonate yielding from magnesium hydroxide and CO_2 gas reactions. The main objectives were to find oxygen mass transfer coefficient as a function of physical parameters, like rotation speed and feed rate of CO_2. The volumetric mass transfer coefficient [k_La] of oxygen was calculated based on absorption experiments. The rotation speed varied from 235 to 465 rpm and its effect on saturation of oxygen into the solution was calculated. Three types of solutions were used: pure water, water-quartz suspension and water-calcium carbonate suspension. The achieved saturation was mainly 95% or more, in case of water maximum value of k_La and P/V was 0.014s^{-1} and 2400 W/m^3. Quartz slurry gave almost the same value of k_La, i.e. 0.04 s^{-1} with P/V of 2450 W/m^3.

For calcium carbonate, the particle concentration was varied from 17.4 g to 2382 g along with two size fractions: 1) particles with average size of 5 µm and 2) size fraction classified with 45 and 63 µm sieves. The behavior of 17.4 g $CaCO_3$ slurry with particle size of 5µm and 45-63µm was almost the same, and obtained k_La and P/V were 0.016 s^{-1} and 2400 W/m^3, respectively. However, when concentration of $CaCO_3$ is increased to 69.9 g, the k_La value is 0.014 $s^{-1}$with particle size of 5 µm and 0.017 s^{-1} with particle size of 45 to 63 µm. Further increase in concentration of calcium carbonate, i.e. 870g and 2382 W/m^3 does not affect volumetric mass transfer coefficient of oxygen. It could be concluded from absorption results that maximum value of k_La is 0.016 s^{-1}. Also particle size and concentration does affect the transfer rate to some extends.

For investigating kinetics when magnesium hydroxide reacts with CO_2 gas, precipitation experiments were performed. The constant concentration of $Mg(OH)_2$ was 100 g, the rotation speed varied from 560 to 750 rpm, whereas the used feed rates of CO_2 were 1 and 9 L/min. With560 rpm andCO_2 feed rate of 1 L/min, the maximum value of Mg ion and TC were 0.25 mol/litre and 0.12 mol/litre with the residence time of 40 min. When flow rate of CO_2 was increased to 9 L/min with same 560 rpm, the achieved value of Mg and TC were 0.3 mol/litre and 0.12 mol/L with shorter residence time of 30 min.

At higher 650 or 750 rpm rotation speeds with 1 L/min feed rate of CO_2, it was observed that the dissociation of magnesium hydroxide is low and small value of Mg ion concentration is achieved, i.e. 0.08 mol/litres. Hence, TC is also low 0.09 mol/litres and therefore, it is concluded that feed rate of CO_2 is dominant in precipitation experiments and it has a key role in dissociation and reaction of magnesium hydroxide with CO_2 gas yielding magnesium carbonate precipitate.

8. References

1. Agency, U.S.E.P. Sources of Greenhouse gases Emission. 2013 [cited 2014 02.01.2014]; Available from: http://www.epa.gov/climatechange/ghgemissions/sources/electricity.html.
2. International Energy Agency, CO_2 Emission from Fuel Combustion in 2012: France.
3. Paul Alivisatos, Basic Research Needs for Carbon Capture beyond 2020, Lawrence Berkeley National Laboratory, Michelle Buchanan, 2010, Oak Ridge National Laboratory. p. 7-25.
4. Gregory T.Benz, Piloting Bioreactor for Agitation Scale-Up, 2008,Benz Technology International, Process Development Symposium 2008.
5. CRC, C., Post-Combustion Capture of Carbon dioxide, CO_2 CRC: Australia.
6. M.Giulietti, M.M.S., S.Derenzo1, M.I.Re and E. Cekinski Industrial Crystallization and Precipitation from Solutions: State of Technique. Brazilian Journal of Chemical Engineering, 2001. 18(4).
7. Danckwerts, P.V., The Absorption of Gases in Liquids, University of Cambridge UK.
8. Dang, H., CO_2 Absorption Rate and Solubility in Monoethanolamine/Piperazine/Water, in First National Conference on Carbon Sequestration, 2001: Washington, DC.
9. Anca Loana Hienola, On the Homogeneous and Heterogeneous Nucleation of Some Organic Compounds, PhD Thesis in Faculty of Science 2008, University of Helsinki: Finland.
10. Nucleation and Spinodal Decomposition 2011, MIT: USA.
11. Schmelzer, J.W.P., Nucleation Theory and Application Wiley-VCH, 2005: p. 76-86.
12. Vekilov, James J. De Yoreo and Peter G. Vekilov, Principles of Crystal Nucleation and Growth Mineralogy and Geochemistry. 54: p. 57-93.
13. D. O Grady, M.B., E. Casey and B. Glennon, The Effect of Mixing on the Metastable Zone Width and Nucleation Kinetics in the Anti-Solvent Crystallization of Benzoic Acid. . Institution of Chemical Engineers, 2007(School

of Chemical and Biochemical Engineering, University College Dublin, Belfield, Dublin, Ireland.).

14. S. Mostafa Noweea, A.A., Jose A. Romagnolib., Antisolventcrystallization:Model identification, experimental validation anddynamic simulation. Chemical Engineering Science, 2008. 63: p. 5457 - 5467.
15. Hsien-Hsin Tung, E.L.P., Michael Midler, and James A. McCauley, Crystallization of Organic Compounds: An Industrial Perspective. Wiley, 2009: p. 207-235.
16. Joao F.Cajaiba da Silva, Andreia P. M. da Silva and Rodrigo C. de Sena, Real-Time Analysis to Evaluate Crystallization Processes. (Instituto de Química – Universidade Federal do Rio de Janeiro, Brazil).
17. S. Nollet,C.Hilgers and J.L Urai, Experimental study of polycrystal growth from an advecting supersaturated fluid in a model fracture. Geofluids 2006. 6(Geologie-Endogene Dynamik, RWTH Aachen, Aachen, Germany): p. 185-200.
18. Paul A.Larsen, Daniel B. Patience and James B.Rawlings, Manupilating Crystal size, Shape and Structure. IEEE Control System Magazine, 2006.
19. Marika Torbacke, On the Influence of Mixing and Scale up in Semi-Batch Reaction Crystallization, PhD Thesis in Department of Chemical Engineering and Technology2001, KTH: Sweden.
20. Marie Ståhl, Marie Ståhl, Åke C. Rasmuson, Towards predictive simulation of single feed semibatch reaction crystallization. Chemical Engineering Science, 2009. 64: p. 1559 - 1576.
21. Sreepriya Vedantam and Vivek V Ranade, Crystallization: Key thermodynamic, kinetic and hydrodynamic aspects. Indian Academy of Sciences, 2013. 38: p. 1287–1337.
22. Valiulin,Karasev, V. V.Komarovskikh, Yu Baklanov, An experimental method for studying the heterogeneous nucleation in a laminar flow chamber. Atmospheric and Oceanic Optics, 2012. 25(6): p. 451-456.
23. Pietsch, W., Agglomeration in Industry. Wiley-VCH-Verlag, 2005.
24. A. Mersmann, Crystallization Technology Handbook. 2001: CRC Press. 527-580.

25. Wang, Yongli, Ma.Shuyuan, Lü. Xiaodong Xie, and Chuang, Control of the agglomeration of crystals in the reactive crystallization of 5-(difluoromethoxy)-2-mercapto-1H-benzimidazole. Frontiers of Chemical Science and Engineering, 2012. 6(4): p. 423-431.
26. Jones, A.G., Crystallization Process Systems. 2002: Butterworth Heinemann.
27. P. K. Kulkarni, M.D., Ashwini G Kini and M.Karthik Preparation and characterization of spherical agglomerates of Ibuprofen by solvent change method. Scholars Research Library, 2010. 5: p. 289-301.
28. Beckmann, W., Crystallization: Basic Concepts and Industrial Applications. Wiley-VCH,2013.
29. Elizabeth Allen, P.S., Jim Henshaw, A Review of Particle Agglomeration, US Department of Energy, AEA Technology, 2001.
30. Brunsteiner, M., Interactions Between Crystal Surfaces in Solution and Agglomeration | a Theoretical Approach, 2003, University of London: London.
31. Richard G.Holdich, Fundamental of Particle Technology. 2002, Loughborough University: UK.
32. Pokrovsky, O.S., Precipitation of Calcium and Magnesium Carbonates from Homogeneous Supersaturated Solution. Journal of Crystal Growth 1998. 186: p. 233-239.
33. Kralj, L.B.a.D., On Calcium Carbonates: From Fundamental Research to Application. Croatica Chemica Acta, 2007. 80(3-4): p. 467-484.
34. Qiao Zhang, Shu-Juan Liu and Shu-Hong Yu, Recent advances in oriented attachment growth and synthesis of functional materials: concept, evidence, mechanism, and Future. Journal of Materials Chemistry, 2009. 19(2): p. 173-312.
35. Myerson, A., Handbook of Industrial Crystallization. 2002, Butterworth-Heinemann: GB. p. 141-161.
36. Mullin, J., Crystallization. 2001, Butterworth-Heinemann: UK. p. 315.
37. Wojtowics, J.A., Factors Affecting Precipitation of Calcium Carbonate Journal of Swimming pool and Spa Industry 2001. 3(1): p. 18-28.

38. Mariz, Dan G. Chapel and Carl L. Mariz, Recovery of CO_2 from Flue Gases: Commercial Trends. Canadian Society of Chemical Engineers annual meeting, 1999: p. 1-13.

39. Robert Socolow, M.D., Roger Aines,Jason Blackstock, Jennifer Wilcox, Direct Air Capture of CO_2 with Chemicals, in A Technology Assessment for the APS Panel on Public Affairs2011, American Physical Society

40. Sean I. Plasynski and Zhong-Ying Chen, Review of CO_2 Capture Technologies and Some Important Opportunities., US DOE National Energy Technology Laboratory and Science Applications International Corporation.

41. IECM Technical Documentation: Membrane-based CO_2 Capture Systems for Coal-fired Power Plants, 2012, Carnegie Mellon University: USA.

42. Intergovernmental Panel on Climate Change, Carbon Dioxide Capture and Storage, UNEP. p. 120-122.

43. Maroto-Valer, M.M., Developments and Innovation in Carbon Dioxide (CO2) Capture and Storage Technology in Carbon Dioxide (CO_2) Capture ,Transport and Industrial Application. WoodHead. p. 220-222.

44. Piet N.L Lens, Christian Kennes, Pierre Le Cloirec and Marc A.Deshusses, Waste Gas Treatment for Resource Recovery. 2006, London,UK: IWA. 415-420.

45. Guangxi Yue, Hai Zhang, Changsui Zhao, Zhongyang Luo, Proceedings of the 20th International Conference on Fluidized Bed Combustion 2009. Beijing, China: Tsinghua University Press and Springer.

46. Joong Beom Lee, T.H.E., Bok Seok Oh, Jeom-In Baek, Jungho Ryu, Won Sik Jeon, Young Ho Wi, Chong Kul Ryu, CO_2 capture from flue gas using potassium-based dry regenerable sorbents. Energy Procedia, 2011. 4: p. 1494-1499.

47. N. Rodríguez*, N. Rodríguez*, M. Alonso andJ. C. Abanades, Experimental investigation of a circulating fluidized-bed reactor to capture CO_2 with CaO. AIChE Journal, 2011. 57(5): p. 1356-1366.

48. Chong Kul Ryu, Joong Beom Lee, Tae Hyoung Eom, Je Myung Oh, and Chang Keun Yi, Development of Na and K-Based Sorbents for CO2 Capture from Flue Gas in Fourth Annual Conference on Carbon Capture and Sequestration DOE/NETL 2005.

Appendix A Calculation Tables of Absorption

Table 4 Absorption of oxygen in $CaCO_2$ suspension (69.6 g, 5 µm). Here N is rotation per minutes(rpm), Q is flow rate in litres/min, T is temperature in Celcius, U is conductivity, t_0 and t_f are initial and final time in minute, C_o andC_f are initial and final concentration is mg/l, S_0 and S_f are initial and final saturation, kLa is oxygen mass transfer coefficient, and P is power in volts.

N	Q	T	U	t_0	C_0	S_0	t_f	C_f	S_f	Kla	F_p	P	P/V
235	6	10	1.37	15:28	0.39	3.5	15:38	10.75	95.0	0.00484	0.813467	20.00857	229.9836
235	6	10	1.37	15:52	0.33	2.8	16:02	10.75	95.0	0.004834	0.813467	20.00857	229.9836
296	6	10	2.52	16:11	0.33	3.0	16:18	10.71	95.1	0.007251	1.494692	46.30756	532.2708
296	6	10	2.52	16:30	0.35	3.1	16:37	10.79	95.1	0.006981	1.494692	46.30756	532.2708
367	6	10	4.11	16:45	0.30	2.7	16:50	10.77	95.0	0.009913	2.436561	93.59479	1075.802
367	6	10	4.11	16:58	0.26	2.3	17:03	10.79	95.2	0.010246	2.436561	93.59479	1075.802
417	6	10	5.36	17:11	0.27	2.4	17:15	10.78	95.2	0.013137	3.177023	138.6644	1593.843
417	6	10	5.36	17:22	0.53	4.7	17:26	10.81	95.4	0.013448	3.177023	138.6644	1593.843
464	6	10	6.80	17:35	0.28	2.5	17:39	10.78	95.0	0.01454	4.030036	195.72	2249.656
464	6	10	6.80	17:45	0.28	2.5	17:49	10.79	95.3	0.014343	4.030036	195.72	2249.656

Table 5 Absorption of oxygen in $CaCO_3$ suspension (174 g, 5 µm)

N	Q	T	U	t_0	C_0	S_0	t_f	C_f	S_f	Kla	F_p	P	P/V
238	6	10	1.49	18:15	0.33	2.9	18:25	10.81	95.0	0.005033	0.884551	22.03476	253.2731
238	6	10	1.49	18:35	0.36	3.2	18:45	10.79	95.0	0.005135	0.884551	22.03476	253.2731
296	6	10	2.52	18:54	0.36	3.2	19:01	10.82	95.3	0.007187	1.494692	46.30756	532.2708
296	6	10	2.52	19:15	0.36	3.2	19:22	10.81	95.0	0.007149	1.494692	46.30756	532.2708
364	6	10	4.05	19:30	0.34	3.0	19:35	10.78	95.1	0.010362	2.401019	91.4756	1051.444
364	6	10	4.05	19:42	0.33	2.9	19:47	10.78	95.1	0.010105	2.401019	91.4756	1051.444
418	6	10	5.52	19:55	0.33	2.9	19:59	10.78	95.1	0.013602	3.271802	143.1435	1645.328
418	6	10	5.52	20:06	0.41	3.6	20:10	10.77	95.0	0.013821	3.271802	143.1435	1645.328
466	6	10	6.79	20:18	0.32	2.8	20:22	10.83	95.4	0.016875	4.024112	196.2747	2256.031
466	6	10	6.79	20:29	0.35	3.1	20:33	10.82	95.5	0.017077	4.024112	196.2747	2256.031

Table 6 Absorption of oxygen in $CaCO_3$ suspension (69.6 g, 45-63 µm)

N	Q	T	U	t_0	C_0	S_0	t_f	C_f	S_f	Kla	F_p	P	P/V
464	6	10	6.70	18:08	0.40	3.6	18:11	10.84	95.3	0.017358	3.970799	192.8432	2216.588
464	6	10	6.70	18:18	0.35	3.2	18:21	10.79	95.0	0.016953	3.970799	192.8432	2216.588
418	6	10	5.47	18:27	0.39	3.5	18:31	10.78	95.0	0.013528	3.242184	141.8477	1630.433
418	6	10	5.44	18:37	0.35	3.1	18:41	10.79	95.2	0.013785	3.224413	141.0702	1621.497
365	6	10	4.11	18:47	0.42	3.7	18:52	10.84	95.4	0.01061	2.436561	93.08474	1069.94
365	6	10	4.10	18:58	0.45	4.0	19:03	10.84	95.4	0.010875	2.430637	92.85844	1067.338
298	6	10	2.57	19:11	0.57	5.0	19:17	10.85	95.4	0.007346	1.524311	47.54427	546.4859
298	6	10	2.57	19:24	0.46	4.1	19:30	10.82	95.2	0.00734	1.524311	47.54427	546.4859
238	6	10	1.54	19:39	0.50	4.4	19:48	10.82	95.0	0.004977	0.91417	22.77258	261.7538
238	6	10	1.54	19:57	0.51	4.5	20:05	10.82	95.1	0.005273	0.91417	22.77258	261.7538

Table 7 Absorption of oxygen in $CaCO_3$ suspension (174 g, 45-63 µm)

N	Q	T	U	t_0	C_0	S_0	t_f	C_f	S_f	Kla	F_p	P	P/V
236	6	10	1.47	13:16	0.42	3.7	13:24	10.78	95.1	0.005129	0.872704	21.55695	247.781
236	6	10	1.48	13:34	0.44	3.9	13:42	10.77	95.0	0.005208	0.878628	21.70327	249.4629
296	6	10	2.51	13:52	0.38	3.4	13:58	10.81	95.3	0.007203	1.488769	46.12404	530.1614
296	6	10	2.51	14:05	0.42	3.7	14:11	10.81	95.3	0.007319	1.488769	46.12404	530.1614
366	6	10	4.01	15:30	0.39	3.5	15:34	10.83	95.2	0.010764	2.377324	91.07052	1046.788
366	6	10	4.05	15:41	0.35	3.1	15:46	10.81	95.4	0.010666	2.401019	91.97822	1057.221
418	6	10	5.45	15:53	0.43	3.9	15:47	10.69	95.3	0.014383	3.230337	141.3294	1624.476
418	6	10	5.39	16:03	0.39	3.5	16:07	10.70	95.6	0.014052	3.194794	139.7744	1606.602
466	6	10	6.79	16:16	0.38	3.4	16:19	10.83	95.6	0.017571	4.024112	196.2747	2256.031
466	6	10	6.75	16:25	0.44	3.9	16:28	10.77	95.0	0.017562	4.000418	195.119	2242.747

Table 8 Absorption of oxygen in $CaCO_3$ suspension (870 g, 45-63 µm)

N	Q	T	U	t_0	C_0	S_0	t_f	C_f	S_f	Kla	F_p	P	P/V
464	6	10	6.77	16:53	0.37	3.3	16:56	10.84	95.2	0.016959	4.012265	194.857	2239.735
464	6	10	6.75	17:02	0.43	3.8	17:05	10.83	95.3	0.017105	4.000418	194.2816	2233.122
418	6	10	5.47	17:13	0.40	3.6	17:17	10.83	95.4	0.013709	3.242184	141.8477	1630.433
418	6	10	5.44	17:23	0.43	3.8	17:27	10.84	95.4	0.013587	3.224413	141.0702	1621.497
365	6	10	4.01	17:34	0.39	3.4	17:39	10.81	95.0	0.010322	2.377324	90.82169	1043.927
365	6	10	4.02	17:45	0.35	3.1	17:50	10.79	95.1	0.010629	2.383247	91.04799	1046.529
298	6	10	2.59	17:57	0.37	3.3	18:03	10.82	95.1	0.007341	1.536158	47.9138	550.7334
298	6	10	2.60	18:11	0.34	3.0	18:17	10.82	95.1	0.007347	1.542082	48.09857	552.8571
236	6	10	1.48	18:27	0.34	3.0	18:36	10.83	95.2	0.004996	0.878628	21.70327	249.4629
236	6	10	1.48	18:46	0.40	3.6	18:55	10.82	95.0	0.005158	0.878628	21.70327	249.4629

Table 9 Absorption of oxygen in $CaCO_3$ suspension (2382 g, 45-63 µm)

N	Q	T	U	t_0	C_0	S_0	t_f	C_f	S_f	Kla	F_p	P	P/V
236	6	10	1.47	14:14	0.44	3.9	14:22	10.80	95.1	0.005025	0.872704	21.55695	247.781
236	6	10	1.48	14:31	0.43	3.9	14:39	10.80	95.1	0.005046	0.878628	21.70327	249.4629
296	6	10	2.54	14:47	0.47	4.2	14:53	10.79	95.1	0.007248	1.50654	46.67461	536.4898
296	6	10	2.55	15:00	0.38	3.4	15:06	10.83	95.5	0.007216	1.512464	46.85814	538.5993
365	6	10	4.01	15:13	0.46	4.1	15:17	10.84	95.6	0.010529	2.377324	90.82169	1043.927
365	6	10	4.00	15:24	0.49	4.3	15:28	10.83	95.6	0.010588	2.3714	90.59538	1041.326
419	6	10	5.48	15:35	0.53	4.7	15:39	10.85	95.7	0.01385	3.248108	142.4468	1637.32
419	6	10	5.48	15:45	0.44	3.9	15:48	10.76	95.0	0.013996	3.248108	142.4468	1637.32
464	6	10	6.77	15:55	0.35	3.7	15:58	10.84	95.7	0.016471	4.012265	194.857	2239.735
464	6	10	6.71	16:04	0.44	3.1	16:07	10.80	95.5	0.016941	3.976723	193.1309	2219.895

Appendix B Calculation Tables for Precipitation Experiments

Table 10 Molar concentration of species over time with rotation speed of 560 rpm and CO_2 feed rate of 1 L/min, the table is splitted into two parts for better visualization. Here V_1 is volume of acid used for phenolphthalein(FF), V_2 volume of acid used for methyl orange(MO), V_3 is the sum of V_1 and V_2.

Titration						
Sample	Time	Acid	V_{sample}	V_1	V_2	v3
1	5	0.2	10	1.9	4.3	6.2
2	10	0.2	10	2.9	7.3	10.2
3	15	0.2	10	5.9	12.5	18.4
4	20	0.2	10	4.2	19.1	23.3
5	25	0.2	10	6.0	19.2	25.2
6	30	0.2	10	11.8	23.5	35.3
7	35	0.2	10	6.9	31.2	38.1
8	40	0.2	10	11.9	34.5	46.4
9	45	0.2	10	10.5	30	40.5
10	50	0.2	10	9	34.1	43.1

FF	2FF	MO	mo/ff	hco4	co4	oh	tc	Mg	Mg/1000
0.08837209	0.17674419	0.13870968	2ff>mo	0	0.05033758	0.03803451	0.050338	18.6558	0.018656
0.07945205	0.15890411	0.14313725	2ff>mo	0	0.0636852	0.01576685	0.063685	40.4466	0.040447
0.0944	0.1888	0.13586957	2ff>mo	0	0.04146957	0.05293043	0.04147	86.7220	0.086722
0.04397906	0.08795812	0.1639485	2ff<mo	0.07599038	0.04397906	0	0.119969	116.7630	0.116763
0.0625	0.125	0.15238095	2ff<mo	0.02738095	0.0625	0	0.089881	124.5927	0.124593
0.10042553	0.20085106	0.13314448	2ff>mo	0	0.03271894	0.06770659	0.032719	176.4451	0.176445
0.04423077	0.08846154	0.16377953	2ff<mo	0.07531799	0.04423077	0	0.119549	191.7645	0.191764
0.06898551	0.13797101	0.1487069	2ff<mo	0.01073588	0.06898551	0	0.079721	233.8741	0.233874
0.07	0.14	0.14814815	2ff<mo	0.00814815	0.07	0	0.078148	210.6008	0.210601
0.05278592	0.10557185	0.15823666	2ff<mo	0.05266481	0.05278592	0	0.105451	208.1374	0.208137

Table 11 Species concentrations over time with 560 rpm and 9 L/min CO_2 feed rate, the table is split into two for better visual.

Titration						
Sample	**Time**	**Acid(N HCL)**	**$V_{sample(ml)}$**	**$V_{1(ml)}$**	**$V_{2(ml)}$**	**v3**
1	5	0.2	10	2.1	10.7	12.8
2	10	0.2	10	8.3	16.8	25.1
3	15	0.2	10	7.8	29.0	36.8
4	20	0.2	10	9.8	35.2	45.0
5	25	0.2	10	7.2	44.2	51.4
6	30	0.2	10	11.5	44.1	55.6
7	35	0.2	10	15.9	37.0	52.9
8	40	0.2	10	8.1	15.65	23.8
9	45	0.2	10	6.3	13.7	20.0
10	50	0.2	10	8.45	8.35	16.8

FF	2FF	MO	mo/ff	hco3	co3	oh	tc	Mg	Mg/1000
0.0328125	0.065625	0.1671875	2ff<mo	0.1015625	0.0328125	0	0.134375	55.3204	0.0553204
0.06613546	0.13227092	0.13386454	2ff=mo	0	0.06613546	0	0.06613546	119.757	0.119757
0.0423913	0.08478261	0.1576087	2ff<mo	0.07282609	0.0423913	0	0.11521739	199.602	0.199602
0.04355556	0.08711111	0.15644444	2ff<mo	0.06933333	0.04355556	0	0.11288889	236.4313	0.2364313
0.02804284	0.05608569	0.17195716	2ff<mo	0.11587147	0.02804284	0	0.14391431	269.9131	0.2699131
0.04122412	0.08244824	0.15877588	2ff<mo	0.07632763	0.04122412	0	0.11755176	291.9398	0.2919398
0.06017029	0.12034059	0.13982971	2ff<mo	0.01948912	0.06017029	0	0.07965941	257.343	0.257343
0.06821053	0.13642105	0.13178947	2ff>mo	0	0.06357895	0.00463158	0.06357895	201.3339	0.2013339
0.063	0.126	0.137	2ff<mo	0.011	0.063	0	0.074	162.2307	0.1622307
0.10059524	0.20119048	0.09940476	ff=mo	0	0	0.09940476	0	132.2695	0.1322695

Table 12 Precipitation with 650 rpm and 1 L/min CO_2 feed rate, the table is split into two for better visual.

Titration						
Sample	**Time**	**Acid**	**V_{sample}**	**V_1**	**V_2**	**v3**
1	10	0.1	10	16.4	44.5	60.9
2	20	0.1	10	24.0	92.3	116.3
3	30	0.1	10	25.0	126.7	151.7
4	40	0.1	10	14.5	101.1	115.6
5	50	0.1	10	6.5	107.2	113.7

v3	FF	2FF	MO	mo/ff	hco4	co4	oh	Tc
60.9	0.02692939	0.05385878	0.07307061	2FF<MO	0.01921182	0.02692939	0	0.046141
116.3	0.02063629	0.04127257	0.07936371	2FF<MO	0.03809114	0.02063629	0	0.058727
151.7	0.01647989	0.03295979	0.08352011	2FF<MO	0.05056032	0.01647989	0	0.06704
115.6	0.01254325	0.02508651	0.08745675	2FF<MO	0.06237024	0.01254325	0	0.074913
113.7	0.0057168	0.0114336	0.0942832	2FF<MO	0.0828496	0.0057168	0	0.088566

Table 13 Precipitation with 750 rpm and 1 L/min CO_2 feed rate, the table is split into two for better visual.

Titration						
Sample	**Time**	**Acid**	**V_{sample}**	**V_1**	**V_2**	**v3**
1	5	0.2	5	0.9	1.9	2.8
2	10	0.2	5	1.6	4.0	5.6
3	15	0.2	5	2.2	6.0	8.2
4	20	0.2	5	3.3	7.4	10.7
5	25	0.2	5	3.9	9.3	13.2
6	30	0.2	5	5.6	9.1	14.7
7	35	0.2	5	6.8	7.3	14.1
8	40	0.2	5	5.7	6.6	12.3
9	45	0.2	5	4.2	7.5	11.7
10	50	0.2	5	5.5	6.4	11.9

FF	2FF	MO	mo/ff	hco4	co4	oh	tc	mg	mg/1000	c analyse	tc ana/1000
0.06666667	0.13333333	0.13333333	2ff=mo	0.13333333	0	0	0.133333	13.8250	0.0138	12.93	0.01293
0.07017544	0.14035088	0.12982456	2ff>mo	0	0.05964912	0.01052632	0.059649	28.9299	0.0289	26.65	0.02665
0.05287356	0.10574713	0.14712644	2ff<mo	0.04137931	0.05287356	0	0.094253	46.0836	0.0461	37.47	0.03747
0.0626087	0.12521739	0.1373913	2ff<mo	0.01217391	0.0626087	0	0.074783	61.0780	0.0611	51.03	0.05103
0.07714286	0.15428571	0.12285714	2ff>mo	0	0.04571429	0.03142857	0.045714	74.4315	0.0744	63.625	0.063625
0.09882353	0.19764706	0.10117647	2ff>mo	0	0.00235294	0.09647059	0.002353	90.8065	0.0908	73.805	0.073805
0.09265537	0.18531073	0.10734463	2ff>mo	0	0.01468927	0.0779661	0.014689	95.8416	0.0958	81.295	0.081295
0.10470588	0.20941176	0.09529412	2ff>mo	0	-0.0094118	0.11411765	-0.00941	90.5370	0.0905	76.13	0.07613
0.12236842	0.24473684	0.07763158	2ff>mo	0	-0.0447368	0.16710526	-0.04474	81.7339	0.0817	71.97	0.07197
0.14029851	0.28059701	0.05970149	2ff>mo	0	-0.080597	0.22089552	-0.0806	72.2843	0.0723	63.81	0.06381